



# Fermi National Accelerator Laboratory

FERMILAB-Pub-90/111-A  
May 1990

## THE DYNAMIC INSTABILITY OF ADIABATIC BLASTWAVES

DONGSU RYU

NASA/Fermilab Astrophysics Center, Fermilab

and

ETHAN T. VISHNIAC<sup>†</sup>

Department of Astronomy, University of Texas

### ABSTRACT

Adiabatic blastwaves, which have a total energy injected from the center,  $E \propto t^q$ , and propagate through a preshock medium with a density,  $\rho_E \propto r^{-\omega}$ , are described by a family of similarity solutions. Previous work has shown that adiabatic blastwaves with increasing or constant postshock entropy behind the shock front are susceptible to an oscillatory instability, caused by the difference between the nature of the forces on the two sides of the dense shell behind the shock front. This instability sets in if the dense postshock layer is sufficiently thin. In this paper, we consider the stability of adiabatic blastwaves with a decreasing postshock entropy. Such blastwaves, if they are decelerating, always have a region behind the shock front which is subject to convection. Some accelerating blastwaves also have such region, depending on the values of  $q$ ,  $\omega$ , and  $\gamma$  where  $\gamma$  is the adiabatic index. However, since the shock interface stabilizes dynamically induced perturbations, blastwaves become convectively unstable only if the convective zone is localized around the origin or a contact discontinuity far from the shock front. On the other hand, the contact discontinuity of accelerating blastwaves is subject to a strong Rayleigh-Taylor instability. The frequency spectra of the nonradial, normal modes of adiabatic blastwaves have been calculated. The results have been applied to the shocks propagating through supernovae envelopes. We show that the metal/He and He/H interfaces are strongly unstable against the Rayleigh-Taylor instability. This instability will induce mixing in supernovae envelopes. In addition we discuss the implications of this work for the evolution of planetary nebulae.

*Subject headings:* hydrodynamics - instabilities - interstellar: matter - nebulae: planetary - shock waves - stars: supernovae

<sup>†</sup> Submitted to *Astrophysical Journal*

<sup>‡</sup> Presidential Young Investigator and Sloan Fellow



## I. INTRODUCTION

An understanding of the propagation of shock waves in astrophysical systems can be essential for understanding the history and present state of such systems. A blast shock wave (or a blastwave, in short) is generated, by an object releasing energy, whether impulsively, as in a supernova explosion, or continuously, as in a stellar or galactic wind. The resulting blastwave can be described by a Sedov-Taylor type similarity solution, provided the total injected energy  $E$  is a power law in time,

$$E = E_o \left( \frac{t}{t_o} \right)^q, \quad (1.1)$$

and the density of the ambient medium is a power law in radius,

$$\rho_E = \rho_o \left( \frac{r}{r_o} \right)^{-\omega} \quad (1.2)$$

(Sedov 1946, 1959; Taylor 1950; Ostriker and McKee 1988). The similarity formalism demands that the flow quantities depend only on a single dimensionless parameter involving length and time scales. Such a similarity formalism provides an excellent approximation to realistic systems, when it is applied in the region far from the spatial and temporal boundaries and when it contains an adequate description of physics.

The stability of blastwaves has been a longstanding problem to physicists and astrophysicists alike. Erpenbeck (1962) studied the stability of a steady plane-parallel shock dividing space into two homogeneous regions and showed that it is not exponentially unstable against a rippling of the shock front. Subsequently, several workers, including Bertschinger (1986), demonstrated that the shock interface is stable against dynamically induced perturbations because of the stabilizing tangential velocity in the postshock flow, produced by the obliquity of the rippled shock. However, the contact discontinuity between the ejected material and the swept-up gas resembles the classical illustration of a Rayleigh-Taylor instability in accelerating blastwaves. In fact, Bernstein and Book (1978) showed that this contact discontinuity in *isentropic* blastwaves is indeed unstable.

Ryu and Vishniac (1987, 1988) analyzed the stability of adiabatic blastwaves propagating through a uniform medium ( $\omega = 0$ ) and derived the eigenvalues and eigenfunctions for the nonradial, normal modes. Such blastwaves are susceptible to an oscillatory instability, due to the difference between the nature of forces on the two sides of the dense shell behind the shock front. They become subject to growing oscillations if the shell is sufficiently thin. The physical mechanism for this instability was first suggested by Vishniac (1983) for an isothermal shell with infinitesimal thickness and later confirmed by Bertschinger (1986). In a subsequent paper, Vishniac and Ryu (1989) gave an analytical derivation of the eigenmodes of

isothermal blastwaves propagating through a uniform medium under the approximation that the evolutionary time scale of the perturbations is much shorter than the evolutionary time scale of the shock itself. From the above work, it can be seen that adiabatic blastwaves with increasing or constant postshock entropy from the shock front, or with

$$\omega \leq \frac{6 - 2q}{2\gamma + (\gamma - 1)q} \quad (1.3)$$

where  $\gamma$  is the adiabatic index (see §II), are overstable for  $\gamma$  sufficiently close to 1. For a realistic shock this condition is usually equivalent to requiring that the postshock gas cool efficiently. In the absence of radiative cooling such shocks will not be subject to these growing oscillations.

However, as pointed out by Bandiera (1984), some adiabatic blastwaves have a region behind the shock front which is subject to convection and may be convectively unstable. The stability of such blastwaves was studied by Chevalier (1976) and Bandiera (1984). Chevalier used the *local* Rayleigh-Taylor criterion to determine the existence of an instability and the dispersion relation for an incompressible fluid under constant gravitational acceleration bounded by rigid boundaries to estimate the growth rate of the perturbations. On the other hand, Bandiera used the *local* Schwarzschild criterion and a dispersion relation based on a *local* stability analysis. Unfortunately, in this case, convection is driven dynamically, not thermally, and such a dynamically driven instability is generally a *global* instability, not a *local* instability. The *global* stability analysis should include the overall dynamics of the blastwaves and the correct boundary conditions, in addition to the local structure of the blastwaves. Therefore the *local* satisfaction of the convection criterion does not necessarily guarantee the existence of a *global* convective instability, and estimates of the growth rate of perturbations based on a *local* stability analysis may be misleading. Here, we call this instability a convective instability, and reserve the name Rayleigh-Taylor instability to indicate the instability in the contact discontinuity (see §II).

In this paper, we consider the stability of adiabatic blastwaves with decreasing entropy behind the shock front, or

$$\omega > \frac{6 - 2q}{2\gamma + (\gamma - 1)q}. \quad (1.4)$$

They are subject to convective or Rayleigh-Taylor instability depending on the values of  $q$ ,  $\omega$ , and  $\gamma$ . This problem is of more than purely formal interest. Realistic astrophysical shocks often occur in the presence of density gradients and may involve the injection of energy over time long compared to the evolutionary time scale of the blastwave. Supernova explosions, where the shock propagates outward through the envelope of a massive star, constitute an example of the former. The ejection of planetary nebulae in the later stages of stellar evolution may be an example of both significant density gradients and continuous energy injection. In this case, earlier stellar winds may lead to a significant, but rapidly decreasing, density enhancement around the star. Moreover, the planetary nebula itself is probably driven by a

continuous, high-intensity stellar wind. Under these circumstances, instabilities may result in global inhomogeneities in the blastwaves at late times. An equally important effect is the tendency of these instabilities to drive mixing in otherwise chemically distinct layers in the postshock gas.

In this paper we have calculated the frequency spectra of the nonradial, normal modes of adiabatic blastwaves using a method similar to that used in Ryu and Vishniac (1987, 1988). In §II of this paper we have reviewed the Sedov-Taylor type similarity solutions for adiabatic blastwaves. In §III the perturbation equations are derived, and in §IV the boundary conditions at the shock front and at the contact discontinuity or the origin are discussed. In §V the numerical scheme used to solve the perturbation equations is described and the results are discussed. In §VI the results are applied to the shock propagating through the supernova envelopes. Finally, in §VII we discuss the application of our results to the evolution of planetary nebulae.

## II. BLASTWAVES

We treat the postshock fluid as a one-component ideal fluid with an adiabatic index  $\gamma$ . The flow is governed by the usual conservation equations:

$$\frac{\partial \rho}{\partial t} + \vec{\nabla} \cdot (\rho \vec{v}) = 0, \quad (2.1)$$

$$\rho \frac{\partial \vec{v}}{\partial t} + \rho (\vec{v} \cdot \vec{\nabla}) \vec{v} + \vec{\nabla} p = 0, \quad (2.2)$$

$$\frac{\partial p}{\partial t} + \vec{v} \cdot \vec{\nabla} p + \gamma p \vec{\nabla} \cdot \vec{v} = 0. \quad (2.3)$$

The energy conservation equation can be replaced by the entropy conservation equation

$$\left( \frac{\partial}{\partial t} + \vec{v} \cdot \vec{\nabla} \right) \ln \frac{p}{\rho^\gamma} = 0 \quad (2.4)$$

except at the shock discontinuity. The shock is assumed to be very strong, so that the fluid density, velocity, and pressure just behind the shock front are expressed in terms of the preshock density  $\rho_E$  and the shock velocity  $V_s$  relative to the preshock medium

$$\rho_s = \rho_E \frac{\gamma + 1}{\gamma - 1}, \quad (2.5)$$

$$v_s = \frac{2V_s}{\gamma + 1}, \quad (2.6)$$

$$p_s = \frac{2\rho_E V_s^2}{\gamma + 1}, \quad (2.7)$$

by the shock jump conditions. The flow pattern is entirely determined by two quantities,  $\rho_E$  and  $E$ , and from them a unique dimensionless parameter of similarity flow can be formed,

$$\begin{aligned}\xi &= r \left( \frac{\rho E}{Et^2} \right)^{1/5} \\ &= \left( \frac{\rho_o r_o^\omega t_o^q}{E_o} \right)^{1/5} r^{\frac{5-\omega}{5}} t^{-\frac{2+q}{5}}.\end{aligned}\quad (2.8)$$

The radius and velocity of the shock front change as

$$r_s \propto t^{\frac{2+q}{5-\omega}}, \quad (2.9)$$

$$V_s \propto t^{-\frac{3-\omega-q}{5-\omega}}, \quad (2.10)$$

and the fluid density, velocity, and pressure just behind the shock front change as

$$\rho_s \propto t^{-\frac{\omega(2+q)}{5-\omega}}, \quad (2.11)$$

$$v_s \propto t^{-\frac{3-\omega-q}{5-\omega}}, \quad (2.12)$$

$$p_s \propto t^{-\frac{\omega q - 2q + 6}{5-\omega}}. \quad (2.13)$$

It is convenient to introduce the dimensionless fluid density, velocity, and pressure, and the dimensionless radial coordinate for the flow throughout the region behind the shock front as defined by

$$\bar{\rho} \equiv \frac{\rho}{\rho_s}, \quad (2.14)$$

$$\bar{v} \equiv \frac{v}{v_s}, \quad (2.15)$$

$$\bar{p} \equiv \frac{p}{p_s}, \quad (2.16)$$

$$\bar{r} \equiv \frac{r}{r_s}. \quad (2.17)$$

Then, the conservation equations (2.1), (2.2), and (2.4) become

$$\left( \frac{2}{\gamma+1} \bar{v} - \bar{r} \right) \frac{1}{\bar{\rho}} \frac{d\bar{\rho}}{d\bar{r}} + \frac{2}{\gamma+1} \frac{d\bar{v}}{d\bar{r}} + \frac{4}{\gamma+1} \frac{\bar{v}}{\bar{r}} - \omega = 0, \quad (2.18)$$

$$\left( \frac{2}{\gamma+1} \bar{v} - \bar{r} \right) \frac{d\bar{v}}{d\bar{r}} + \frac{\gamma-1}{\gamma+1} \frac{1}{\bar{\rho}} \frac{d\bar{p}}{d\bar{r}} - \frac{3-\omega-q}{2+q} \bar{v} = 0, \quad (2.19)$$

$$-\gamma \left( \frac{2}{\gamma+1} \bar{v} - \bar{r} \right) \frac{1}{\bar{\rho}} \frac{d\bar{\rho}}{d\bar{r}} + \left( \frac{2}{\gamma+1} \bar{v} - \bar{r} \right) \frac{1}{\bar{p}} \frac{d\bar{p}}{d\bar{r}} - \left( \frac{6-2q+\omega q}{2+q} - \gamma\omega \right) = 0. \quad (2.20)$$

Blastwaves with  $\omega < 5$  admit a similarity solution where the radius and velocity of the shock front remain finite, even though the total mass and energy contained in a blastwave is infinite if  $\omega \geq 3$ .

For  $q = 0$  the above equations can be integrated analytically. The integration is given in Sedov (1959), and also in Bandiera (1984) in a compact form. Blastwaves with  $q = 0$  are *filled*, i.e. the postshock flow extends to the origin, provided  $\omega < (7 - \gamma)/(\gamma + 1)$ . In this case, near the origin, the density becomes

$$\bar{\rho} \propto \bar{r}^{\frac{3-\gamma\omega}{\gamma-1}}, \quad (2.21)$$

and the pressure approaches a constant value with

$$\frac{d\bar{p}}{d\bar{r}} \propto \bar{r}^{\frac{2+\gamma-\gamma\omega}{\gamma-1}}. \quad (2.22)$$

On the other hand, blastwaves with  $q = 0$  are *hollow*, i.e. the postshock flow ends at a contact discontinuity, provided  $\omega > (7 - \gamma)/(\gamma + 1)$ . In this case, near the contact discontinuity, the density and pressure become

$$\bar{\rho} \propto (\bar{r} - \bar{r}_c)^{\frac{6-(\gamma+1)\omega}{3\gamma-6+\omega}}, \quad (2.23)$$

$$\bar{p} \propto (\bar{r} - \bar{r}_c)^{\frac{3\gamma-\gamma\omega}{3\gamma-6+\omega}}. \quad (2.24)$$

Here,  $\bar{r}_c$  is the position of the contact discontinuity. The special case with  $\omega = (7 - \gamma)/(\gamma + 1)$  is sometimes referred as the Primakoff blastwave, and the postshock fluid quantities are expressed by a simple power law in radius:

$$\bar{\rho} \propto \bar{r}, \quad (2.25)$$

$$\bar{p} \propto \bar{r}^3. \quad (2.26)$$

The blastwaves with  $q = 0$  can be classified into 7 characteristic types depending on the values of  $\omega$  and  $\gamma$ , and the ranges of  $\omega$  for each type are given in Bandiera (1984). The plots of the postshock flow for each characteristic type of the blastwaves with  $\gamma = 4/3$  are shown in Figure 2 of Chevalier (1976).

For  $q > 0$  equations (2.18), (2.19), and (2.20) can not be integrated analytically, but the behavior of the postshock flow can be induced from the equations. All the blastwaves with  $q > 0$  are *hollow*. Near the contact discontinuity,

$$\begin{aligned} \frac{\bar{r} - \bar{r}_c}{\bar{\rho}} \frac{d\bar{\rho}}{d\bar{r}} &\propto \frac{6 - 2q + \omega q}{2 + q} - \gamma\omega && \text{for } \omega \leq 3 \\ \frac{\bar{r} - \bar{r}_c}{\bar{\rho}} \frac{d\bar{\rho}}{d\bar{r}} &< 0 && \text{for } \omega > 3. \end{aligned} \quad (2.27)$$

The density converges to zero or a constant if

$$\omega \leq \frac{6 - 2q}{2\gamma + (\gamma - 1)q}, \quad (2.28)$$

and diverges otherwise. Also near the contact discontinuity,

$$\frac{1}{\bar{\rho}} \frac{d\bar{p}}{d\bar{r}} \propto 3 - \omega - q, \quad (2.29)$$

and the pressure approaches a constant value if  $\omega < 3$  and diverges otherwise. On the other hand, near the shock front,

$$\frac{d\bar{p}}{d\bar{r}} \propto 6(3 - q) - 4 \frac{\gamma - 1}{\gamma + 1} (2 + q) - [2(2 + \gamma) + (\gamma - 1)q]\omega, \quad (2.30)$$

$$\frac{d\bar{p}}{d\bar{r}} \propto 2(2\gamma - 1)(3 - q) - 4\gamma \frac{\gamma - 1}{\gamma + 1} (2 + q) - [2\gamma - (\gamma - 1)q]\omega. \quad (2.31)$$

(The above relations also hold for the cases with  $q = 0$ .) The blastwaves with  $q > 0$  can be classified into 5 characteristic types depending on the values of  $q$ ,  $\omega$ , and  $\gamma$ , and the ranges of  $\omega$  for each type are following:

figure (a)

$$\omega < \frac{6 - 2q}{2\gamma + (\gamma - 1)q}, \quad (2.32)$$

figure (b)

$$\frac{6 - 2q}{2\gamma + (\gamma - 1)q} < \omega < \frac{6(3 - q)}{2(2 + \gamma) + (\gamma - 1)q} - \frac{\gamma - 1}{\gamma + 1} \frac{4(2 + q)}{2(2 + \gamma) + (\gamma - 1)q}, \quad (2.33)$$

figure (c)

$$\begin{aligned} & \frac{6(3 - q)}{2(2 + \gamma) + (\gamma - 1)q} - \frac{\gamma - 1}{\gamma + 1} \frac{4(2 + q)}{2(2 + \gamma) + (\gamma - 1)q} < \omega \\ & < \frac{2(2\gamma - 1)(3 - q)}{2\gamma - (\gamma - 1)q} - \frac{\gamma - 1}{\gamma + 1} \frac{4\gamma(2 + q)}{2\gamma - (\gamma - 1)q}, \end{aligned} \quad (2.34)$$

figure (d)

$$\frac{2(2\gamma - 1)(3 - q)}{2\gamma - (\gamma - 1)q} - \frac{\gamma - 1}{\gamma + 1} \frac{4\gamma(2 + q)}{2\gamma - (\gamma - 1)q} < \omega < 3 - q, \quad (2.35)$$

and figure (e)

$$3 - q < \omega < 5. \quad (2.36)$$

Figure 1 shows the plots of the postshock flow for each characteristic type of the blastwaves with  $\gamma = 5/3$  and  $q = 1$ . Each plot is meant to illustrative of a range of values of  $\omega$  which yield similar results.

It is well known that a region is subject to a convective motion if the entropy increases in the direction of gravity (see, for example, Landau and Lifshitz 1959). Denoting by  $S$  the entropy per unit mass, which is defined as

$$S \equiv \ln \left( \frac{\bar{p}}{\bar{\rho}^\gamma} \right), \quad (2.37)$$

it can be seen from equation (2.20) that the entropy increases or stays constant from the shock front toward the origin or the contact discontinuity provided

$$\omega \leq \frac{6 - 2q}{2\gamma + (\gamma - 1)q}, \quad (2.38)$$

and decreases otherwise. On the other hand, even though we are neglecting gravity, the presence of a pressure gradient implies the flow is accelerated and gives rise to an effective gravity

$$g_{eff} \equiv -\frac{1}{\bar{\rho}} \frac{d\bar{p}}{d\bar{r}}. \quad (2.39)$$

The postshock region around the contact discontinuity is decelerated (or accelerated in the direction of increasing entropy) provided

$$\omega < 3 - q \quad (2.40)$$

(see equation (2.29)), and the postshock region behind the shock front is decelerated provided

$$\omega < \frac{2(2\gamma - 1)(3 - q)}{2\gamma - (\gamma - 1)q} - \frac{\gamma - 1}{\gamma + 1} \frac{4\gamma(2 + q)}{2\gamma - (\gamma - 1)q} \quad (2.41)$$

(see equation (2.31)). Hence, all or a portion of postshock region is subject to a convective motion if

$$\begin{aligned} & \frac{6 - 2q}{2\gamma + (\gamma - 1)q} < \omega \\ & < \max\left[(3 - q), \frac{2(2\gamma - 1)(3 - q)}{2\gamma - (\gamma - 1)q} - \frac{\gamma - 1}{\gamma + 1} \frac{4\gamma(2 + q)}{2\gamma - (\gamma - 1)q}\right]. \end{aligned} \quad (2.42)$$

In such region, the *local* strength of the convective motion may be estimated by the *local* growth rate given by Bandiera (1984),

$$\sigma = \sqrt{g_{eff} \frac{dS}{d\bar{r}}}. \quad (2.43)$$

From equations (2.18), (2.19), and (2.20), it can be seen that  $\sigma^2$  approaches a constant near the origin in filled blastwaves, or if

$$q = 0 \quad \text{and} \quad \omega \leq \frac{7 - \gamma}{\gamma + 1}, \quad (2.44)$$

and  $\sigma^2 \propto 1/(r - r_c)$  near the contact discontinuity in the hollow blastwaves, or if

$$q > 0 \quad \text{or} \quad q = 0 \quad \text{and} \quad \omega > \frac{7 - \gamma}{\gamma + 1}. \quad (2.45)$$

Hence, if convection occurs in the postshock flow, it is expected to be highly localized in hollow blastwaves but not in filled blastwaves. However, the question whether the blastwaves *locally* subject to a convective motion become dynamically unstable is a different problem, as discussed in §I. Since the shock interface stabilizes dynamically

induced perturbations, we expect that only those blastwaves with a highly localized convective zone far from the shock interface, or with

$$\begin{aligned} \frac{7-\gamma}{\gamma+1} < \omega \leq 3 \quad \text{and} \quad q = 0 \\ \text{or} \quad \frac{6-2q}{2\gamma+(\gamma-1)q} < \omega \leq q-3 \quad \text{and} \quad q > 0, \end{aligned} \quad (2.46)$$

are convectively unstable.

The accelerating contact discontinuity with

$$\omega > 3 - q \quad (2.47)$$

and the decelerating shock front with

$$\omega < \frac{2(2\gamma-1)(3-q)}{2\gamma-(\gamma-1)q} - \frac{\gamma-1}{\gamma+1} \frac{4\gamma(2+q)}{2\gamma-(\gamma-1)q} \quad (2.48)$$

have configurations subject to the Rayleigh-Taylor instability. However, again since the shock front tends to suppress the instability, we expect that only those blastwaves with the accelerating contact discontinuity are subject to the Rayleigh-Taylor instability, i.e. only those blastwaves where the instability is localized near the contact discontinuity and far from the shock front.

In the following sections, we will provide a proof of these arguments and find the relevant frequency spectra by performing a linear stability analysis.

### III. PERTURBATION EQUATIONS

In this paper we will follow the notation used in Ryu and Vishniac (1987, 1988) except that  $\omega$  and  $q$  have been added to the list of parameters.

Let  $\delta\tilde{\rho}$ ,  $\delta\tilde{\mathbf{v}}$ , and  $\delta\tilde{p}$  be the normalized, perturbed variables defined in the Eulerian coordinates as

$$\delta\tilde{\rho}(r, \theta, \phi, t) \equiv \frac{\rho(r, \theta, \phi, t) - \rho_o(r, t)}{\rho_s}, \quad (3.1)$$

$$\delta\tilde{\mathbf{v}}(r, \theta, \phi, t) \equiv \frac{\mathbf{v}(r, \theta, \phi, t) - v_o(r, t)\hat{r}}{v_s}, \quad (3.2)$$

$$\delta\tilde{p}(r, \theta, \phi, t) \equiv \frac{p(r, \theta, \phi, t) - p_o(r, t)}{p_s}, \quad (3.3)$$

where  $\rho_o$ ,  $v_o$ , and  $p_o$  are the unperturbed fluid quantities considered in the previous section. Then, by linearizing the hydrodynamic conservation equations (2.1), (2.2), and (2.3) about the perturbed variables, we obtain the perturbation equations

$$\frac{\gamma+1}{2} \frac{5-\omega}{2+q} t \frac{\partial \delta\tilde{\rho}}{\partial t} - \frac{\gamma+1}{2} \omega \delta\tilde{\rho} + \tilde{v} \frac{\partial \delta\tilde{\rho}}{\partial \tilde{r}} + \frac{\partial \tilde{v}}{\partial \tilde{r}} \delta\tilde{\rho} + 2 \frac{\tilde{v}}{\tilde{r}} \delta\tilde{\rho} + \tilde{\rho} \tilde{\nabla} \cdot \delta\tilde{\mathbf{v}} + \frac{\partial \tilde{\rho}}{\partial \tilde{r}} \delta\tilde{v}_r = 0, \quad (3.4)$$

$$\begin{aligned} \frac{\gamma + 15 - \omega}{2} \frac{t}{2 + q} \frac{\partial \delta \bar{v}}{\partial t} - \frac{\gamma + 13 - \omega - q}{2} \frac{\delta \bar{v}}{2 + q} + \bar{v} \frac{\partial \delta \bar{v}}{\partial \bar{r}} + \frac{\partial \bar{v}}{\partial \bar{r}} \delta \bar{v}_r \hat{r} + \frac{\bar{v}}{\bar{r}} \delta \bar{v}_T + \frac{\gamma - 1}{2} \frac{1}{\bar{\rho}} \bar{\nabla} \delta \bar{p} \\ - \frac{\gamma - 1}{2} \frac{1}{\bar{\rho}^2} \frac{\partial \bar{p}}{\partial \bar{r}} \delta \bar{\rho} \hat{r} = 0, \end{aligned} \quad (3.5)$$

$$\frac{\gamma + 15 - \omega}{2} \frac{t}{2 + q} \frac{\partial}{\partial t} \left( \frac{\delta \bar{p}}{\bar{\rho}} - \gamma \frac{\delta \bar{\rho}}{\bar{\rho}} \right) + \bar{v} \frac{\partial}{\partial \bar{r}} \left( \frac{\delta \bar{p}}{\bar{\rho}} - \gamma \frac{\delta \bar{\rho}}{\bar{\rho}} \right) + \left( \frac{1}{\bar{\rho}} \frac{\partial \bar{p}}{\partial \bar{r}} - \gamma \frac{1}{\bar{\rho}} \frac{\partial \bar{\rho}}{\partial \bar{r}} \right) \delta \bar{v}_r = 0, \quad (3.6)$$

where  $\bar{\nabla}$  is the normalized spatial derivative and  $\delta \bar{v}_r$  and  $\delta \bar{v}_T$  are the radial and tangential components of the normalized perturbed velocity.

Since the unperturbed flow is self-similar, we have seen in the previous section that the normalized, unperturbed fluid quantities  $\bar{\rho}$ ,  $\bar{v}$ , and  $\bar{p}$  depend only on a single, normalized, dimensionless radius  $\bar{r}$ . Hence, we assume that the normalized, perturbed variables can be written in a self-similar form consisting of a term which depends only on the normalized radius, the usual expansion in spherical harmonics, and a power law in time:

$$\delta \bar{\rho}(r, \theta, \phi, t) = \sum_{l, m} \delta \bar{\rho}_{lm}(\bar{r}) Y_{lm}(\theta, \phi) t^s, \quad (3.7)$$

$$\delta \bar{v}(r, \theta, \phi, t) = \sum_{l, m} \left[ \delta \bar{v}_{rlm}(\bar{r}) Y_{lm}(\theta, \phi) t^s \hat{r} + \delta \bar{v}_{Tlm}(\bar{r}) \bar{r} \bar{\nabla}_T Y_{lm}(\theta, \phi) t^s \right], \quad (3.8)$$

$$\delta \bar{p}(r, \theta, \phi, t) = \sum_{l, m} \delta \bar{p}_{lm}(\bar{r}) Y_{lm}(\theta, \phi) t^s, \quad (3.9)$$

where the operator  $\bar{\nabla}_T$  is defined as

$$\bar{\nabla}_T \equiv \frac{1}{\bar{r}} \frac{\partial}{\partial \theta} \hat{\theta} + \frac{1}{\bar{r} \sin \theta} \frac{\partial}{\partial \phi} \hat{\phi}. \quad (3.10)$$

Here,  $s$  is the dimensionless perturbation growth rate. It depends on  $l$  and may be either real or a complex number. The first-order perturbation equations, which are the partial differential equations, are reduced to a set of ordinary differential equations:

$$\begin{aligned} \left( \bar{v} - \frac{\gamma + 1}{2} \bar{r} \right) \frac{d \delta \bar{\rho}}{d \bar{r}} + \bar{\rho} \frac{d \delta \bar{v}_r}{d \bar{r}} + \left[ \frac{d \bar{v}}{d \bar{r}} + 2 \frac{\bar{v}}{\bar{r}} - \frac{\gamma + 1}{2} \omega + \frac{\gamma + 15 - \omega}{2} \frac{s}{2 + q} \right] \delta \bar{\rho} \\ + \left[ \frac{d \bar{\rho}}{d \bar{r}} + 2 \frac{\bar{\rho}}{\bar{r}} \right] \delta \bar{v}_r - l(l + 1) \frac{\bar{\rho}}{\bar{r}} \delta \bar{v}_T = 0, \end{aligned} \quad (3.11)$$

$$\begin{aligned} \left( \bar{v} - \frac{\gamma + 1}{2} \bar{r} \right) \bar{\rho} \frac{d \delta \bar{v}_r}{d \bar{r}} + \frac{\gamma - 1}{2} \frac{d \delta \bar{p}}{d \bar{r}} - \frac{\gamma - 1}{2} \frac{1}{\bar{\rho}} \frac{d \bar{p}}{d \bar{r}} \delta \bar{\rho} \\ + \left[ \frac{d \bar{v}}{d \bar{r}} - \frac{\gamma + 13 - \omega - q}{2} \frac{1}{2 + q} + \frac{\gamma + 15 - \omega}{2} \frac{s}{2 + q} \right] \bar{\rho} \delta \bar{v}_r = 0, \end{aligned} \quad (3.12)$$

$$\left(\tilde{v} - \frac{\gamma+1}{2}\tilde{r}\right)\tilde{\rho}\frac{d\delta\tilde{v}_T}{d\tilde{r}} + \left[\frac{\tilde{v}}{\tilde{r}} - \frac{\gamma+1}{2}\frac{3-\omega-q}{2+q} + \frac{\gamma+1}{2}\frac{5-\omega}{2+q}s\right]\tilde{\rho}\delta\tilde{v}_T + \frac{\gamma-1}{2}\frac{1}{\tilde{r}}\delta\tilde{p} = 0, \quad (3.13)$$

$$\begin{aligned} -\gamma\left(\tilde{v} - \frac{\gamma+1}{2}\tilde{r}\right)\frac{d\delta\tilde{p}}{d\tilde{r}} + \left(\tilde{v} - \frac{\gamma+1}{2}\tilde{r}\right)\frac{\tilde{\rho}}{\tilde{p}}\frac{d\delta\tilde{p}}{d\tilde{r}} + \left[-\gamma\frac{1}{\tilde{\rho}}\frac{d\tilde{p}}{d\tilde{r}} + \frac{1}{\tilde{p}}\frac{d\tilde{p}}{d\tilde{r}}\right]\tilde{\rho}\delta\tilde{v}_T \\ + \gamma\left[\left(\tilde{v} - \frac{\gamma+1}{2}\tilde{r}\right)\frac{1}{\tilde{\rho}}\frac{d\tilde{p}}{d\tilde{r}} - \frac{\gamma+1}{2}\frac{5-\omega}{2+q}s\right]\delta\tilde{p} \\ - \left[\left(\tilde{v} - \frac{\gamma+1}{2}\tilde{r}\right)\frac{1}{\tilde{p}}\frac{d\tilde{p}}{d\tilde{r}} - \frac{\gamma+1}{2}\frac{5-\omega}{2+q}s\right]\frac{\tilde{\rho}}{\tilde{p}}\delta\tilde{p} = 0. \end{aligned} \quad (3.14)$$

Here, we have dropped the subscript  $lm$  from  $\delta\rho_{lm}$ ,  $\delta v_{r lm}$ ,  $\delta v_{T lm}$ , and  $\delta p_{lm}$  for clarity. Although we do not distinguish notationally between, say,  $\delta\tilde{p}(r, \theta, \phi, t)$  and  $\delta\tilde{p}(\tilde{r})$ , it is clear that the latter form is applied in the above equations. In deriving the equations (3.11) to (3.14), we have used the relations

$$\frac{\partial\delta\tilde{p}}{\partial t} = -\frac{2+q}{5-\omega}\frac{\tilde{r}}{t}\frac{\partial\delta\tilde{p}}{\partial\tilde{r}} + \frac{s}{t}\delta\tilde{p}, \quad (3.15)$$

$$\frac{\partial\delta\tilde{v}}{\partial t} = -\frac{2+q}{5-\omega}\frac{\tilde{r}}{t}\frac{\partial\delta\tilde{v}}{\partial\tilde{r}} + \frac{s}{t}\delta\tilde{v}, \quad (3.16)$$

$$\frac{\partial\delta\tilde{p}}{\partial t} = -\frac{2+q}{5-\omega}\frac{\tilde{r}}{t}\frac{\partial\delta\tilde{p}}{\partial\tilde{r}} + \frac{s}{t}\delta\tilde{p}. \quad (3.17)$$

## IV. BOUNDARY CONDITIONS

### a) Outer Boundary Conditions

The outer boundary conditions at the shock front for the perturbation equations (3.11) to (3.14) are derived from the requirement of the mass, momentum, and energy flux conservations across the shock front:

$$[\rho u_r] = 0, \quad (4.1)$$

$$[p + \rho u_r^2] = 0, \quad (4.2)$$

$$[u_T] = 0, \quad (4.3)$$

$$\left[\frac{1}{2}u^2 + \frac{\gamma}{\gamma-1}\frac{p}{\rho}\right] = 0. \quad (4.4)$$

Here,  $u_r$  is the fluid velocity relative to and perpendicular to the shock front and  $u_T$  is the fluid velocity parallel to the shock front. The square brackets denote the difference in the enclosed quantities across the shock front.

Let  $\eta_s$  be the perturbation in the position of the shock front,  $r_s$ , and  $\tilde{\eta}_s$  be the normalized perturbation defined as

$$\tilde{\eta}_s(\theta, \phi, t) \equiv \frac{\eta_s(\theta, \phi, t)}{r_s}. \quad (4.5)$$

Following equations (3.7) to (3.10), we assume that  $\tilde{\eta}_s$  can be written as:

$$\tilde{\eta}_s(\theta, \phi, t) = \sum_{l,m} \tilde{\eta}_{slm} Y_{lm}(\theta, \phi) t^s. \quad (4.6)$$

Then, the equations (4.1) to (4.4) give the normalized boundary conditions at the shock front for the perturbation equations (3.11) to (3.14)

$$\delta\tilde{p} = -\tilde{\eta}_s \frac{d\tilde{p}}{d\tilde{r}} - \omega\tilde{\eta}_s, \quad (4.7)$$

$$\delta\tilde{v}_r = -\tilde{\eta}_s \frac{d\tilde{v}}{d\tilde{r}} + \left( \frac{5-\omega}{2+q} s + 1 \right) \tilde{\eta}_s, \quad (4.8)$$

$$\delta\tilde{p} = -\tilde{\eta}_s \frac{d\tilde{p}}{d\tilde{r}} - \omega\tilde{\eta}_s + 2 \left( \frac{5-\omega}{2+q} s + 1 \right) \tilde{\eta}_s, \quad (4.9)$$

$$\delta\tilde{v}_T = -\tilde{\eta}_s, \quad (4.10)$$

where the subscript  $lm$  has been dropped for clarity. We have assumed that the ambient medium is unperturbed in deriving the above conditions. We will set  $\tilde{\eta}_s = 1$  for convenience.

### b) Inner Boundary Conditions

The derivation of the inner boundary conditions is subtler than that of the outer boundary conditions. The physical arguments for the inner boundary conditions are different for *filled* and *hollow* blastwaves. The inner boundary conditions at the origin for *filled* blastwaves, i.e., for

$$q = 0 \quad \text{and} \quad \omega \leq \frac{7-\gamma}{\gamma+1}, \quad (4.11)$$

were considered in Ryu and Vishniac (1987). From the requirement that the fluid should not undergo divergent perturbations in the Lagrangian sense at the origin, or the fractional density change of the displaced volume element should go to zero at the origin, the boundary condition

$$\delta p = 0 \quad (4.12)$$

is obtained. The same boundary condition is also obtained from the requirement that the energy perturbation should vanish at the origin.

The inner boundary conditions at the contact discontinuity for *hollow* blast-waves, i.e, for

$$q > 0 \quad \text{or} \quad q = 0 \quad \text{and} \quad \omega > \frac{7-\gamma}{\gamma+1}, \quad (4.13)$$

were considered in Ryu and Vishniac (1988). They are derived from the requirement that there are no mass, momentum and energy fluxes across the contact discontinuity, or

$$u_r = 0 \quad (4.14)$$

at the contact discontinuity and

$$[p] = 0 \quad (4.15)$$

across the contact discontinuity. Here,  $u_r$  is the fluid velocity relative to and perpendicular to the contact discontinuity. Let  $\eta_c$  be the perturbation in the position of the contact discontinuity,  $r_c$ , and  $\tilde{\eta}_c$  be the normalized perturbation defined as

$$\tilde{\eta}_c(\theta, \phi, t) \equiv \frac{\eta_c(\theta, \phi, t)}{r_s}. \quad (4.16)$$

Then, the above two equations give

$$\delta\tilde{v}_r + \tilde{\eta}_c \frac{d\tilde{v}}{d\tilde{r}} - \frac{\gamma+1}{2} \left( \frac{5-\omega}{2+q} s + 1 \right) \tilde{\eta}_c = 0, \quad (4.17)$$

$$\delta\tilde{p} + \tilde{\eta}_c \frac{d\tilde{p}}{d\tilde{r}} = 0. \quad (4.18)$$

In deriving the above conditions, it has been assumed that there is no perturbation inside the contact discontinuity, where a vacuum forms if  $q = 0$  and  $\omega > (7-\gamma)/(\gamma+1)$  or the sound speed is so large to smooth out immediately all the perturbations if  $q > 0$ . In the case that  $d\tilde{p}/d\tilde{r} = 0$  near the contact discontinuity, or for

$$\begin{aligned} q = 0 & \quad \omega < \frac{6}{\gamma+1} \\ q > 0 & \quad \omega < \frac{6-2q}{2\gamma+(\gamma-1)q}, \end{aligned} \quad (4.19)$$

the second condition becomes

$$\delta\tilde{p} = 0 \quad (4.20)$$

which is completely sufficient as the inner boundary condition. In this case the other one may be used to compute  $\tilde{\eta}_c$ . However, in the case that  $d\tilde{p}/d\tilde{r} \neq 0$  near the contact discontinuity, both conditions must be invoked to obtain a solution.

## V. NUMERICAL SOLUTIONS

The first-order perturbation equations (3.11) to (3.14) with the outer boundary conditions (4.7) to (4.11) and the inner boundary conditions (4.12) or (4.17) and

(4.18) constitute eigenvalue equations for the eigenvalue  $s$ , which we have solved using the following iteration method. First, the derivatives of the normalized, perturbed variables with respect to the dimensionless radius have been calculated from the equations (3.11) to (3.14)

$$\frac{d\delta\vec{Q}}{d\tilde{r}} = \tilde{\mathcal{A}} \cdot \delta\vec{Q}, \quad (5.1)$$

where  $\delta\vec{Q}$  is a vector with

$$\delta\vec{Q} \equiv \begin{pmatrix} \delta\tilde{\rho} \\ \delta\tilde{v}_r \\ \delta\tilde{p} \\ \delta\tilde{v}_T \end{pmatrix} \quad (5.2)$$

and  $\tilde{\mathcal{A}}$  is a  $4 \times 4$  matrix whose elements are functions of  $\tilde{\rho}$ ,  $\tilde{v}$ ,  $\tilde{p}$ ,  $d\tilde{\rho}/d\tilde{r}$ ,  $d\tilde{v}/d\tilde{r}$ ,  $d\tilde{p}/d\tilde{r}$ , and  $\tilde{r}$ . Second, for given values of  $q$ ,  $\omega$ ,  $\gamma$ , and  $l$ , the eigenvalue  $s$  has been estimated. Using the outer boundary conditions at the shock front, the above equation has been integrated numerically up to the origin or to the contact discontinuity. The integration has been carried out using the Runge-Kutta-Verner fifth-order and sixth-order method. In order to improve the accuracy around the origin or the contact discontinuity where some quantities diverge, i)  $\ln \tilde{\rho}$ ,  $\ln \tilde{p}$ , or  $\ln \tilde{r}$  instead of  $\tilde{r}$  has been used as the independent variable and ii) the unperturbed fluid quantities near the origin or the contact discontinuity have been replaced by the leading power-law solutions discussed in §II when possible. Finally, the integrated perturbed quantities at the origin or at the contact discontinuity have checked against the inner boundary conditions. If they have not satisfied the inner boundary conditions,  $s$  has been modified to a better value  $s + \Delta s$  by the formula

$$\Delta s = -\frac{\delta\tilde{p}}{\frac{\partial\delta\tilde{p}}{\partial s}} \quad (5.3)$$

or

$$\Delta s = -\frac{\delta\tilde{v}_r - \frac{d\tilde{v}}{d\tilde{r}} \left(\frac{d\tilde{p}}{d\tilde{r}}\right)^{-1} \delta\tilde{p} + \frac{\gamma+1}{2} \left(\frac{5-\omega}{2+q} s + 1\right) \left(\frac{d\tilde{p}}{d\tilde{r}}\right)^{-1} \delta\tilde{p}}{\frac{\partial\delta\tilde{v}_r}{\partial s} - \frac{d\tilde{v}}{d\tilde{r}} \left(\frac{d\tilde{p}}{d\tilde{r}}\right)^{-1} \frac{\partial\delta\tilde{p}}{\partial s} + \frac{\gamma+1}{2} \left(\frac{5-\omega}{2+q} s + 1\right) \left(\frac{d\tilde{p}}{d\tilde{r}}\right)^{-1} \frac{\partial\delta\tilde{p}}{\partial s} + \frac{\gamma+1}{2} \frac{5-\omega}{2+q} \left(\frac{d\tilde{p}}{d\tilde{r}}\right)^{-1} \delta\tilde{p}}. \quad (5.4)$$

Here,  $\partial\delta\tilde{p}/\partial s$  and  $\partial\delta\tilde{v}_r/\partial s$  have been calculated from

$$\frac{d}{d\tilde{r}} \frac{\partial\delta\vec{Q}}{\partial s} = \frac{\partial\tilde{\mathcal{A}}}{\partial s} \cdot \delta\vec{Q} + \tilde{\mathcal{A}} \cdot \frac{\partial\delta\vec{Q}}{\partial s}. \quad (5.5)$$

The iteration has been continued until  $|\Delta s| \leq 10^{-4}$ , and the resulting  $s$  has been taken as the eigenvalue for given  $q$ ,  $\omega$ ,  $\gamma$ , and  $l$ . Typically,  $s$  converges in 3 or 4 iterations.

In the stability analysis, the blastwaves with  $q = 0$  can be classified into 4 characteristic types, as discussed in §II (refer, for instance, equations (2.38), (2.40),

(2.44), and (2.45)). The ranges of  $\omega$  for which each type applies are given below:  
type (a)

$$\omega \leq \frac{3}{\gamma} \quad \text{and} \quad q = 0, \quad (5.6)$$

type (b)

$$\frac{3}{\gamma} < \omega \leq \frac{7-\gamma}{\gamma+1} \quad \text{and} \quad q = 0, \quad (5.7)$$

type (c)

$$\frac{7-\gamma}{\gamma+1} < \omega \leq 3 \quad \text{and} \quad q = 0, \quad (5.8)$$

type (d)

$$\omega > 3 \quad \text{and} \quad q = 0. \quad (5.9)$$

The plots of the resulting frequency spectra for each characteristic type of blastwaves with  $\gamma = 4/3$  are shown in Figure 2. Each plot is meant to be illustrative of a range in  $\omega$  which yields similar results.

The blastwaves with  $q > 0$  can be classified into 3 characteristic types, and the ranges of  $\omega$  for which each type applies are given below:

type (a)

$$\omega \leq \frac{6-2q}{2\gamma + (\gamma-1)q}, \quad (5.10)$$

type (b)

$$\frac{6-2q}{2\gamma + (\gamma-1)q} < \omega \leq q-3, \quad (5.11)$$

type (c)

$$\omega > q-3. \quad (5.12)$$

The plots of the resulting frequency spectra for each characteristic type of blastwaves with  $\gamma = 5/3$  and  $q = 1$  are shown in Figure 3. Figure 3b actually corresponds to the shock wave structure given in Figure 1c, but the frequency spectra corresponding to perturbations of Figures 1b and 1d are only slightly different. Consequently, we have omitted the corresponding plots and allowed the remaining figure to stand for all three cases.

The frequency spectra of the filled decelerating blastwaves in Figures 2a and 3a are the same frequency spectra as those in Ryu and Vishniac (1987 and 1988) and have been reproduced here for completeness. Such blastwaves are unstable to growing oscillatory modes only when the thickness of the shell behind the shock front is sufficiently thin, or for  $\gamma$  sufficiently close to one.

Blastwaves with  $\omega$  in the range given in (5.7) are apparently subject to a convective motion but have a convective region extending from the origin up to the

shock front. The corresponding frequency spectra, such as Figure 2b, indicate that such blastwaves are actually stable against convection because the shock interface stabilizes the dynamically induced perturbations. On the other hand, blastwaves with  $\omega$  in the ranges given in (5.8) and (5.11) have a convective region highly localized around the contact discontinuity. The corresponding frequency spectra, such as Figures 2c and 3b, indicate that such blastwaves are unstable against the convective instability. In the blastwaves subject to convection, the sound wave modes at long wavelengths bifurcate progressively into growing modes and decaying modes. The first mode to split, which we call the *primary mode*, is also the mode which becomes unstable first. The modes which split at higher  $l$ , which we call the *higher harmonic modes*, become unstable at progressively shorter wavelengths. The primary mode is always the most unstable mode. The bifurcating wavelength,  $k_b$  at which a given mode splits ( $s$  becomes real), and the critical wavenumber,  $k_c$ , at which a given mode becomes unstable ( $s$  becomes positive), depend on the pressure and density distributions in the postshock shell. The detailed dependence of  $k_b$  and  $k_c$  on the internal structure will not be given here, but will be investigated in the subsequent paper (Ryu 1990). In order for the convective instability to be effective, the pressure gradient should be large (see Figure 3b). However, the region initially subject to convection may become less convective as the instability grows, since effect of convection will be to reduce the gradient of the entropy. Clearly, the detailed nonlinear evolution of the convective instability in shocks should be investigated by high-resolution, three-dimensional numerical simulations.

The accelerating contact discontinuity in blastwaves with  $\omega > 3 - q$  is unstable against the Rayleigh-Taylor mode over *all* wavelengths. Figures 2d and 3c show the frequency spectra of a growing mode, which is the only non-oscillatory mode we can identify. Of course, it is expected that there are an infinite number of oscillatory modes corresponding to sound waves propagating throughout the postshock region. However, blastwaves with  $\omega > 3 - q$  are generally stable against such modes over all wavelengths. We have actually identified several such modes but the real part of  $s$  of such modes is always negative. In the subsequent paper (Ryu 1990), we will show that, for perturbations with wavelengths smaller than the thickness of the shell, the growth rate of the Rayleigh-Taylor instability is given by

$$\Gamma \sim \sqrt{gk}, \quad (5.13)$$

where  $g$  is the effective gravity exerted on the shell.

Figure 4 shows the postshock flow of the Primakoff blastwave with  $\gamma = 5/3$ ,  $q = 0$ , and  $\omega = 2$  and its frequency spectra. This is particularly interesting case, since this corresponds to a supernova explosion in a preexisting supersonic stellar wind. Bernstein and Book (1980) considered the the stability of the Primakoff blastwave and showed that it is stable against perturbations on all wavelengths. However, Gaffet (1984a,b) argued that Bernstein and Book had neglected the entropy perturbations and concluded the Primakoff blastwave can be proved to be stable only against radial modes. Our analysis shows that the Primakoff blastwave

is stable also against nonradial, normal modes, even though it is formally subject to a convective motion.

Figure 5 shows the distributions of the perturbed fluid quantities  $\delta\bar{p}$ ,  $\delta\bar{v}_r$ ,  $\delta\bar{p}$ , and  $\delta\bar{v}_T$  of blastwaves which are unstable against the convective instability or the Rayleigh-Taylor instability. The perturbation wavelength corresponds to

$$\begin{aligned}\frac{\lambda}{r_s} &= \frac{2\pi}{l} \\ &= 0.628,\end{aligned}\tag{5.14}$$

which is larger than the thickness of the shells. In both cases, the perturbations are highly localized around the contact discontinuity.

## VI. MIXING IN SUPERNOVA ENVELOPES

The advent of Supernova 1987A in the Large Magellanic Cloud provided the direct observational evidence that hydrodynamic processes may play an important role in the early stage of a supernova explosion. A large scale mixing of the ejecta were suggested from the following observations: i) Both x-ray and  $\gamma$ -ray were discovered earlier than expected (see, *e.g.*, Sunyaev *et al.* 1987; Dotani *et al.* 1987; Matz *et al.* 1988). ii) After a rapid initial decline, the bolometric light curve increased very slowly and then reached a plateau-like maximum (see, *e.g.*, Catchpole *et al.* 1987). iii) Broad lines with FWHM  $v \simeq 2000 - 3000 km s^{-1}$  of Fe II, Ni II, Ar II, and Co II were observed in late 1987 and early 1988 (see, *e.g.*, Erickson *et al.* 1988; Rank *et al.* 1988; Witteborn *et al.* 1989). Several possible mechanisms for mixing were suggested (see Arnett, Fryxell, and Müller 1989 for more discussion and references), and among them some hydrodynamic instability has been considered the most probable solution.

Müller *et al.* (1989) considered the stability of blastwave produced by a point explosion in a  $n = 3$  polytrope and applied the stability analysis of an *incompressible* fluid confined between two *rigid* boundaries discussed in Chandrasekhar (1961). They concluded that the initial perturbations in their model do not grow significantly in the shock propagation time scale. However, Ebisuzaki, Shigeyama, and Nomoto (1989), and Benz and Thielemann (1990) considered the stability of blastwave propagating through a realistic progenitor star and applied a *local* stability analysis based on the Rayleigh-Taylor criterion of an *incompressible* fluid (Ebisuzaki, Shigeyama, and Nomoto) and the Schwarzschild criterion of a compressible fluid (Benz and Thielemann). Both groups concluded that the two composition interfaces between the hydrogen-rich and helium zones and the helium and metal zones are *extremely* unstable. However, as mentioned in §II, an analysis of the dynamic instability of blastwaves should include the overall dynamics, the boundary conditions, and the local background structure. Therefore, estimates of the growth rate of the perturbations based on local criteria may be misleading.

On the other hand, Nagasawa, Nakamura, and Miyama (1988) performed numerical simulations of supernova explosions in  $n = 3$  and  $n = 1.5$  polytropic stars using a three-dimensional smoothed particle hydrodynamic (SPH) code and found the formation of clumpy structures produced by a compressible Rayleigh-Taylor instability. In more accurate numerical simulations using a hydrodynamic code based on the piecewise parabolic method (PPM), Arnett, Fryxell, and Müller (1989) considered a supernova explosion in a realistic progenitor star with  $M = 15M_{\odot}$  by Arnett (1987). They found that the metal/He interface is strongly unstable against the Rayleigh-Taylor instability and heavier metals penetrate into the He zone. On the other hand, they found that the He/H interface stays relatively stable.

We have applied the results of §V to a blastwave propagating through the supernova envelope. The metal/He and He/H interfaces in Ebisuzaki, Shigeyama, and Nomoto (1989) (see their Figures 1 and 2) form contact discontinuities with large density jumps and appear subject to the Rayleigh-Taylor instability, as suggested by Chevalier (1976). As a result, they are expected to be strongly unstable over all wavelengths. However, different models for the supernova progenitor may result in composition interfaces which are stable against the Rayleigh-Taylor instability. The stability of the composition interfaces may be tested by

$$\Sigma = \int_0^t \exp \left[ \text{Re} \left( \sqrt{\frac{1}{\rho} \frac{dp}{dr} k} \right) \right] dt'. \quad (6.1)$$

The growth time scale of the perturbations is comparable to the dynamical time scale of the contact discontinuity for perturbation wavelengths comparable to the thickness of the unstable zone, (at least in the linear regime). Consequently, the long wavelength perturbations will grow about as fast as the supernova explosion evolves. According to the linear stability analysis, perturbations with smaller wavelengths grow faster. However, perturbations with wavelengths smaller than the thickness of the unstable zone are expected to be strongly localized around the composition interfaces. This should prevent them from dominating the long wavelength perturbations. We conclude that the modes that most effectively promote mixing will be the long wavelength modes, i.e. those with wavelengths comparable to the local pressure scale height. On the other hand, the regions between the two composition interfaces and the shock front are expected to be only *weakly*, or *not*, unstable against the convective motions. This is because the small pressure gradient in both regions makes the convective instability ineffective compared to the Rayleigh-Taylor instability of the composition interfaces, and also because convective motions in the region between the He/H interface and the shock front will become stabilized if they extend to the shock front.

## VII. PLANETARY NEBULAE

In the case of a stellar wind driving a shock into its surroundings, it is necessary to take  $q \geq 1$ . For planetary nebulae the standard model is that the bright shell

of ionized material represents a shock being driven into gas which originates from an earlier, and gentler, stellar wind emitted by the same star. When the shock emerges from this neutral material the shock wave will expand rapidly into the low density interstellar medium and the nebula will eventually become less conspicuous. At earlier times the shock will encounter a density gradient that depends on the history of mass loss from the central star. In general, we have  $\omega > 2$ , the value we would have for a steady mass loss at a constant velocity.

In an earlier paper Breitschwerdt and Kahn (1990) have pointed out that under certain reasonable assumptions concerning the evolution of a planetary nebula and its central star the nebula will be subject to the Rayleigh-Taylor instability. They pointed out that this may explain the small scale features seen in most planetary nebulae. This result is consistent with the work we have presented here, but we wish to make a more general point as well. Taking  $q \geq 1$  and  $\omega > 2$  we see immediately from equation (2.48) that we are always in the regime where the contact discontinuity is accelerating and the dense shell is subject to Rayleigh-Taylor instabilities. In particular, we see that this result does not depend on the value of  $\gamma$  in the dense shell (or equivalently, on the importance of radiative cooling). In other words, regardless of the exact model one uses for the evolution for planetary nebulae, the implication of this paper is that small scale instabilities and mixing will necessarily be part of their evolution. Whether this results in large scale features depends on whether or not there are other stabilizing influences at work. For example, a sufficiently intense ionizing flux may stabilize large amplitude ripples in the inner boundary by evaporating lagging dense regions, an effect which is beyond the scope of this paper.

We would like to thank Roger A. Chevalier and Hyesung Kang for comments on manuscripts. The calculations were carried out using facilities of the Minnesota Supercomputer Institute and Fermilab. DR thanks the Minnesota Supercomputer Institute for the hospitality, where some of this work was done. The work of DR was supported in part by the DOE and by NASA at Fermilab through grant NAGW-1340.

*Note* - During the completion of this paper, we received a preprint from J. Goodman. He considered the stability of the blastwaves with  $q = 0$  and  $(7 - \gamma)/(\gamma + 1) < \omega < 3$ . We found that his results agree with ours for that particular case.

## REFERENCES

- Arnett, W. D. 1987, *Ap. J.*, **319**, 136.
- Arnett, W. D., Fryxell, B. A., and Müller, E. 1989, *Ap. J. (Letters)*, **341**, L63.
- Bandiera, R. 1984, *Astr. Ap.*, **139**, 368.
- Benz, W., and Thielemann, F.-K. 1990, *Ap. J. (Letters)*, **348**, L17.
- Bernstein, I. B., and Book, D. L. 1978, *Ap. J.*, **225**, 633.
- . 1980, *Ap. J.*, **240**, 223.
- Bertschinger, E. 1986, *Ap. J.*, **304**, 154.
- Breitschwerdt, D., and Kahn, F. D. 1990, preprint.
- Catchpole, R. M. *et al.* 1987, *M. N. R. A. S.*, **229**, 15p.
- Chandrasekhar, S. 1961, *Hydrodynamic and Hydromagnetic Stability* (Oxford: Clarendon Press).
- Chevalier, R. A. 1976, *Ap. J.*, **207**, 872.
- Dotani, T. *et al.* 1987, *Nature*, **330**, 230.
- Ebisuzaki, T., Shigeyama, T., and Nomoto, K. 1989, *Ap. J. (Letters)*, **344**, L65.
- Erickson, E. F., Haas, M. R., Colgan, S. W. J., Lord, S. D., Burton, M. G., Wolf, J., Hollenbach, D. J., and Werner, M. 1988, *Ap. J. (Letters)*, **330**, L39.
- Erpenbeck, J. J. 1962, *Phys. Fluids*, **5**, 1181.
- Gaffet, B. 1984a, *Ap. J.*, **279**, 419.
- . 1984b, *Astr. Ap.*, **135**, 94.
- Landau, L. D., and Lifshitz, E. M. 1959, *Fluid Mechanics* (New York: Pergamon).
- Matz, S. M., Share, G. H., Leising, M. D., Chupp, E. L., Vestrand, W. T., Purcell, W. R., Strickman, M. S., and Reppin, C. 1988, *Nature*, **331**, 416.

- Müller, E., Hillebrandt, W., Orio, M., Höflich, P., Mönchmeyer, R., and Fryxell, B. A. 1989, *Astr. Ap.*, **220**, 167.
- Nagasawa, M., Nakamura, T., and Miyama, S. M. 1988, *Pub. Astr. Soc. Japan*, **40**, 691.
- Ostriker, J. P., and McKee, C. F. 1988, *Rev. Mod. Phys.*, **60**, 1.
- Rank, D. M. *et al.* 1988, *Nature*, **331**, 505.
- Ryu, D. 1990, in preparation.
- Ryu, D., and Vishniac, E. T. 1987, *Ap. J.*, **313**, 820.
- \_\_\_\_\_. 1988, *Ap. J.*, **331**, 350.
- Sedov, L. I. 1946, *Prikl. Mat. Mekh.*, **10**, 241.
- \_\_\_\_\_. 1959, *Similarity and Dimensional Methods in Mechanics* (New York: Academic).
- Sunyaev, R. *et al.* 1987, *Nature*, **330**, 227.
- Taylor, G. I. 1950, *Proc. Royal Soc. London*, **210A**, 175.
- Vishniac, E. T. 1983, *Ap. J.*, **274**, 152.
- Vishniac, E. T., and Ryu, D. 1989, *Ap. J.*, **337**, 917.
- Witteborn, F. C., Bregman, J. D., Wooden, D. H., Pinto, P. A., Rank, D. M., Woosley, S. E., and Cohen, M. 1989, *Ap. J. (Letters)*, **338**, L9.

## FIGURE CAPTIONS

- Fig. 1.— The characteristic types of the postshock flow of the blastwaves with  $\gamma = 5/3$  and  $q = 1$ . The ranges of  $\omega$  for which each particular type applies are given in the text.
- Fig. 2.— The characteristic types of the frequency spectra of the blastwaves with  $\gamma = 4/3$  and  $q = 0$ . (a) The blastwave with  $\omega = 0$  which is subject to an oscillatory instability but stable against the dynamically induced perturbations. (b) The blastwave with  $\omega = 2.3$  which is subject to a convective motion but stable against the dynamically induced perturbations. (c) The blastwave with  $\omega = 2.7$  which is subject to a convective motion and unstable against the dynamically induced perturbations. (d) The blastwave with  $\omega = 3.2$  which is subject to a Rayleigh-Taylor instability and unstable against the dynamically induced perturbations. The solid lines show the real eigenvalues  $s$  and the dashed lines show the real parts of the complex eigenvalues  $s$ . In (b) and (c), at the points where two solid lines meet, a dashed line starts and extends up to  $l = 1$ . Some dashed lines are omitted for the clarity.
- Fig. 3.— The characteristic types of the frequency spectra of the blastwaves with  $\gamma = 5/3$  and  $q = 1$ . (a) The blastwave with  $\omega = 0$  which is subject to an oscillatory instability but stable against the dynamically induced perturbations. (b) The blastwave with  $\omega = 1.4$  which is subject to a convective motion and unstable against the dynamically induced perturbations. (c) The blastwave with  $\omega = 2.5$  which is subject to a Rayleigh-Taylor instability and unstable against the dynamically induced perturbations. The solid lines show the real eigenvalues  $s$  and the dashed lines show the real parts of the complex eigenvalues  $s$ .
- Fig. 4.— The Primakoff blastwave with  $\gamma = 5/3$ ,  $q = 0$ , and  $\omega = 2$  (a) and its frequency spectra (b). The Primakoff blastwave is subject to a convective motion but stable against the dynamically induced perturbations. The solid lines show the real eigenvalues  $s$  and the dashed lines show the real parts of the complex eigenvalues  $s$ . In (b), at the points where two solid lines meet, a dashed line starts and extends up to  $l = 1$ . Some dashed lines are omitted for the clarity.
- Fig. 5.— The perturbations of the postshock flow. (a) The blastwave with  $\gamma = 4/3$ ,  $q = 0$ , and  $\omega = 2.7$ , which is convectively unstable, for  $l = 10$  and  $s = 0.239$ . (b) The blastwave with  $\gamma = 4/3$ ,  $q = 0$ , and  $\omega = 3.2$ , which is Rayleigh-Taylor unstable, for  $l = 10$  and  $s = 0.713$ .

**Author's Postal Addresses**

Dongsu Ryu:

NASA/Fermilab Astrophysics Center

Fermi National Accelerator Laboratory

MS 209, PO Box 500

Batavia, IL 60510-0500

Ethan T. Vishniac:

Department of Astronomy

University of Texas

Austin, TX 78712

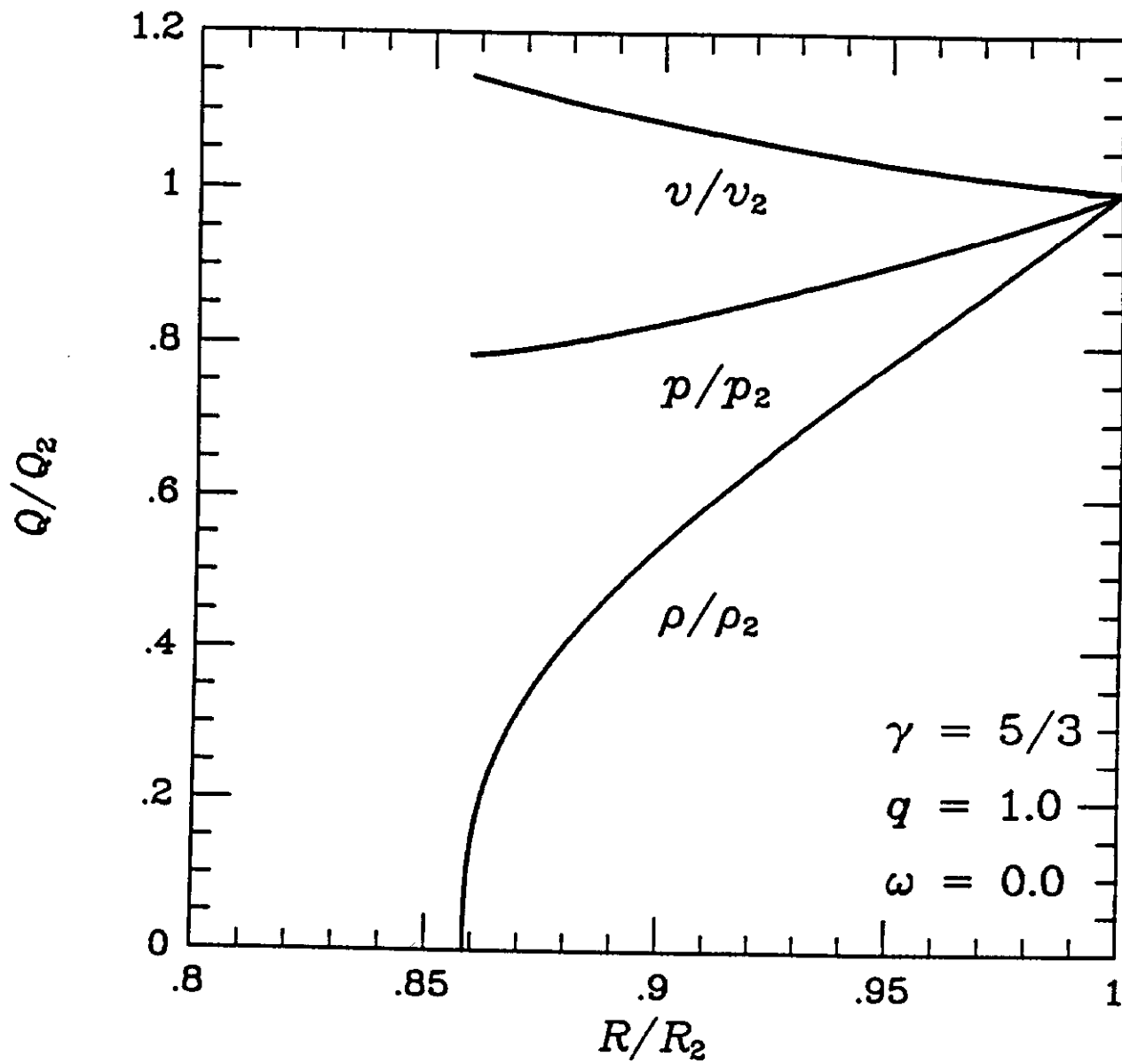


Fig 1 a

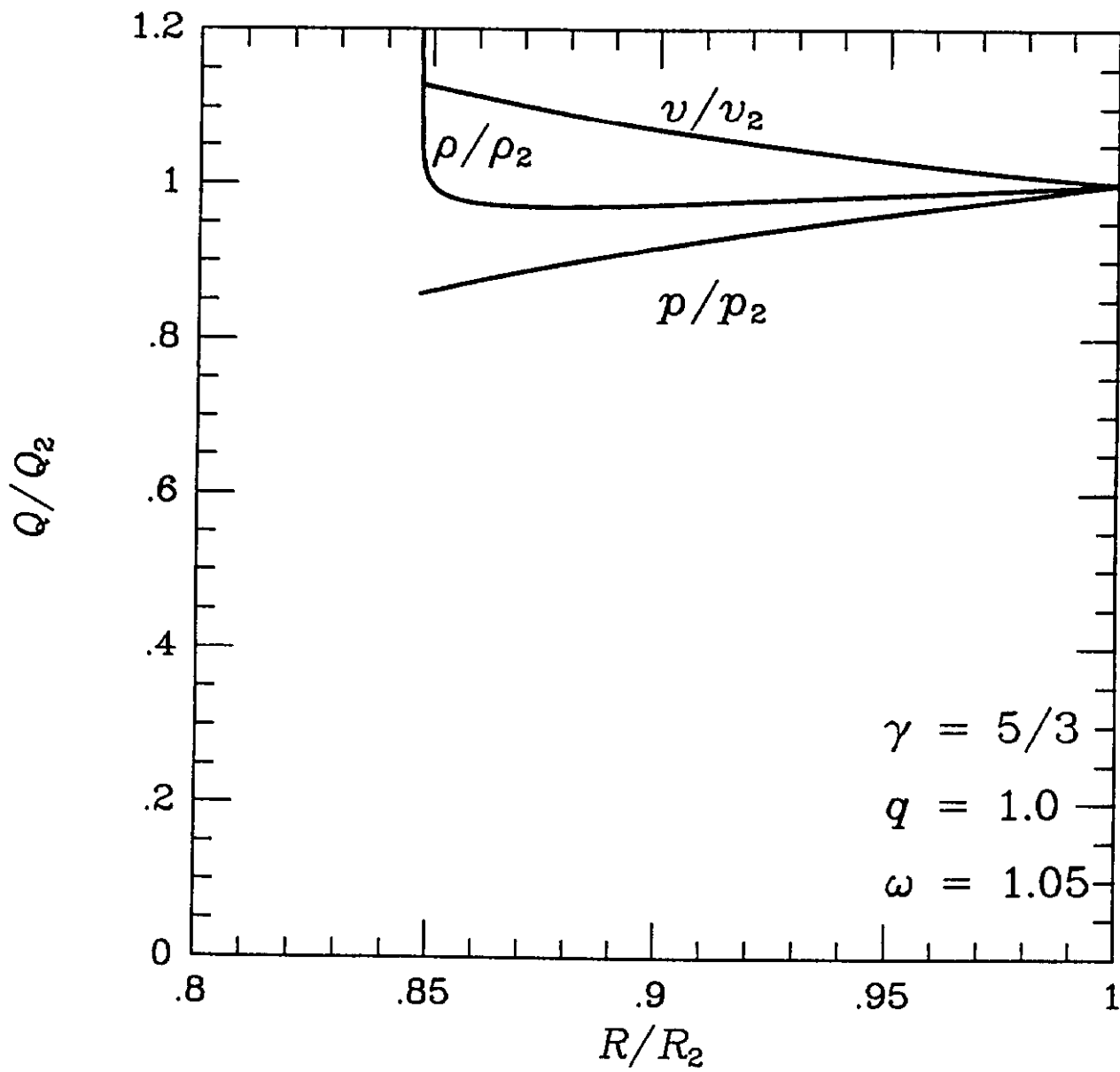


Fig 1b

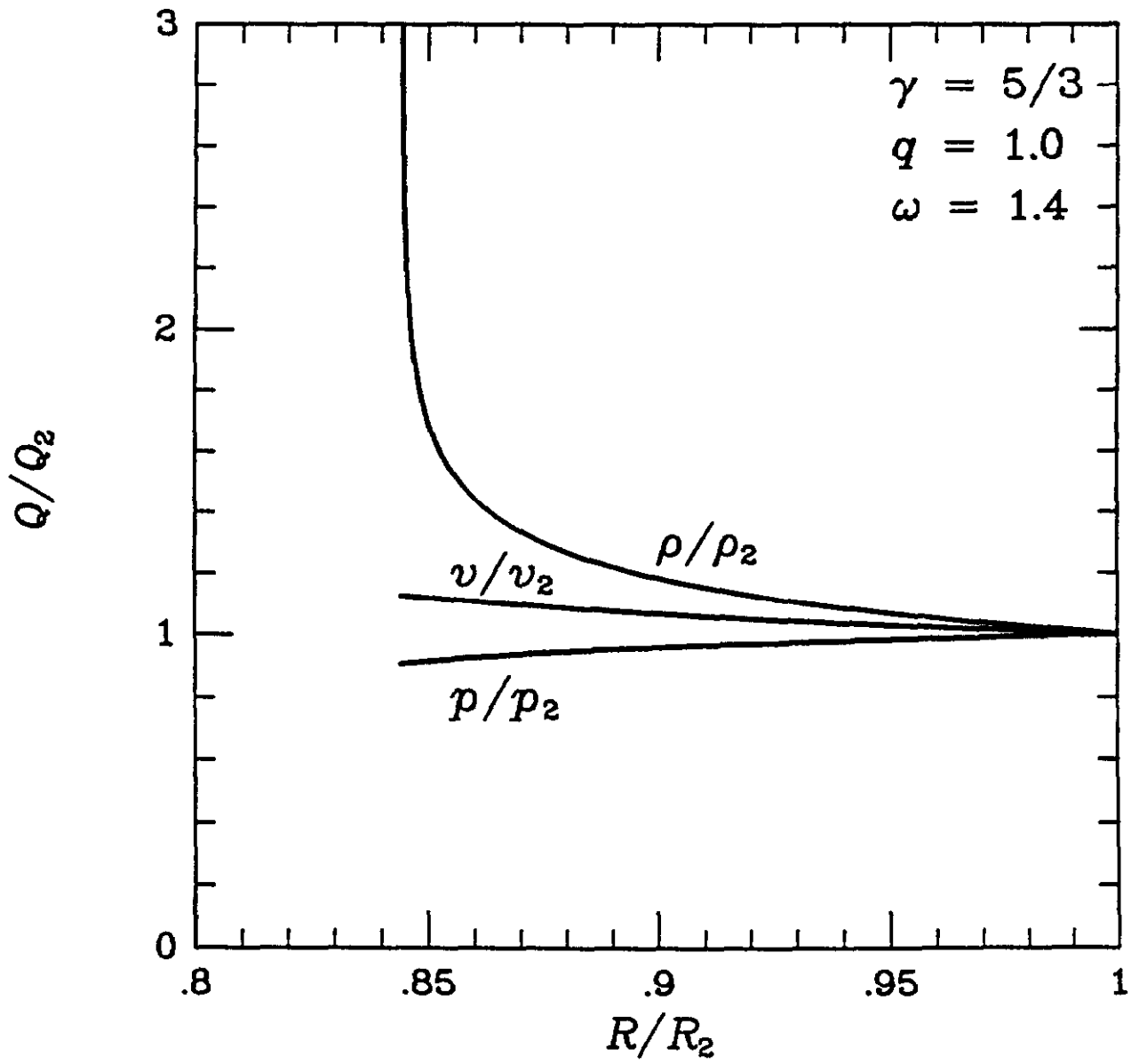


Fig 1c

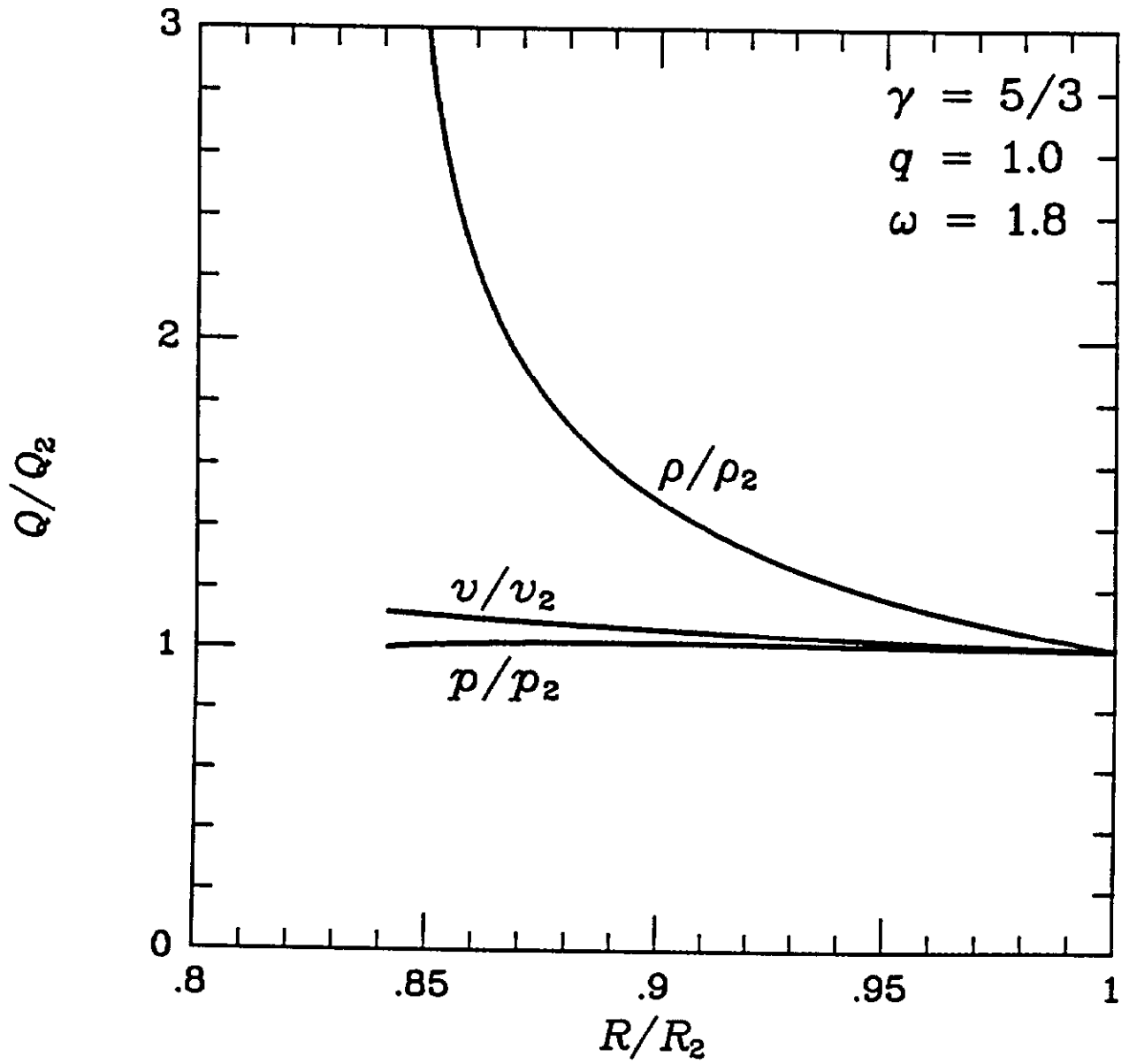


Fig 1d

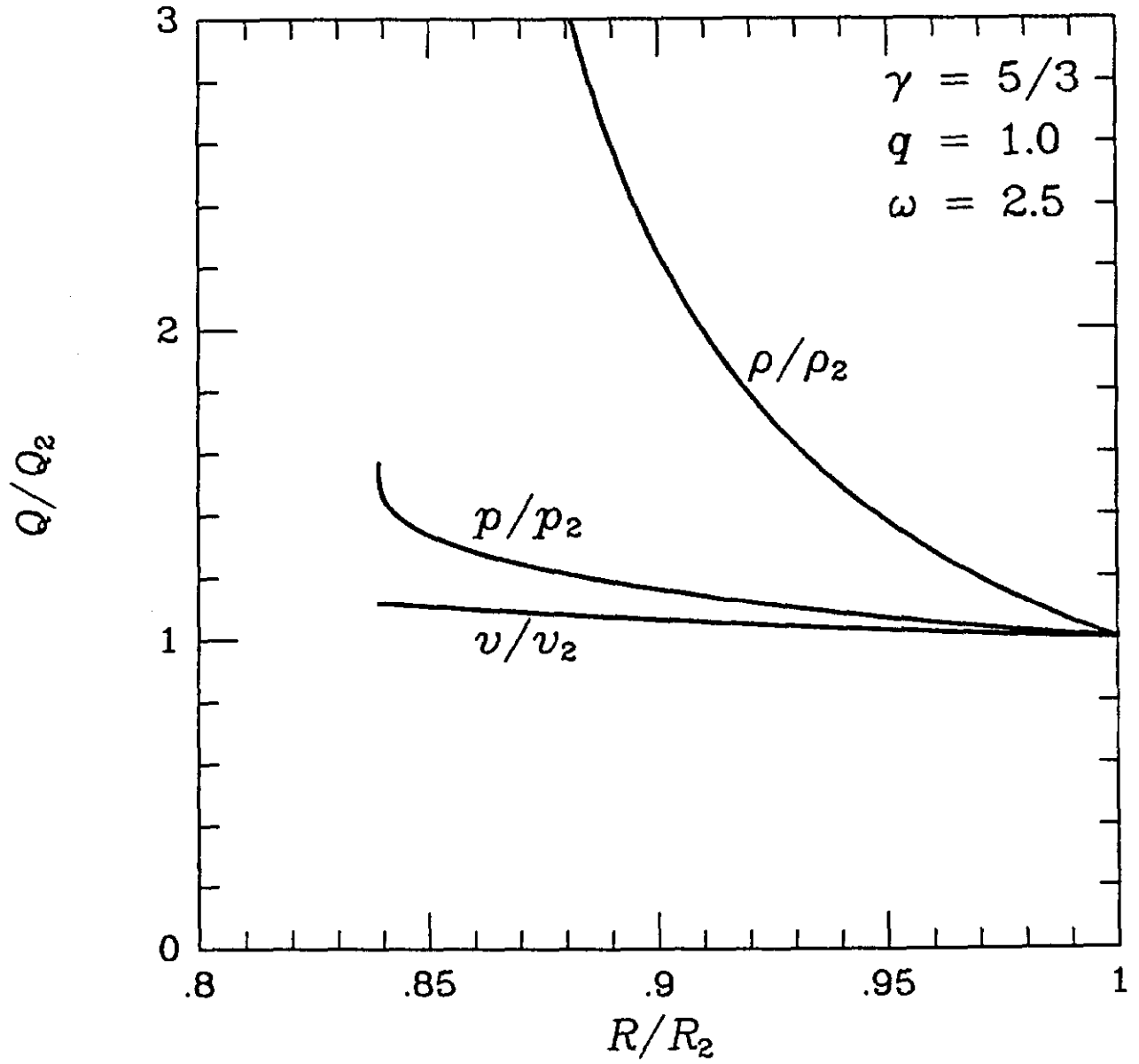


Fig 1 e

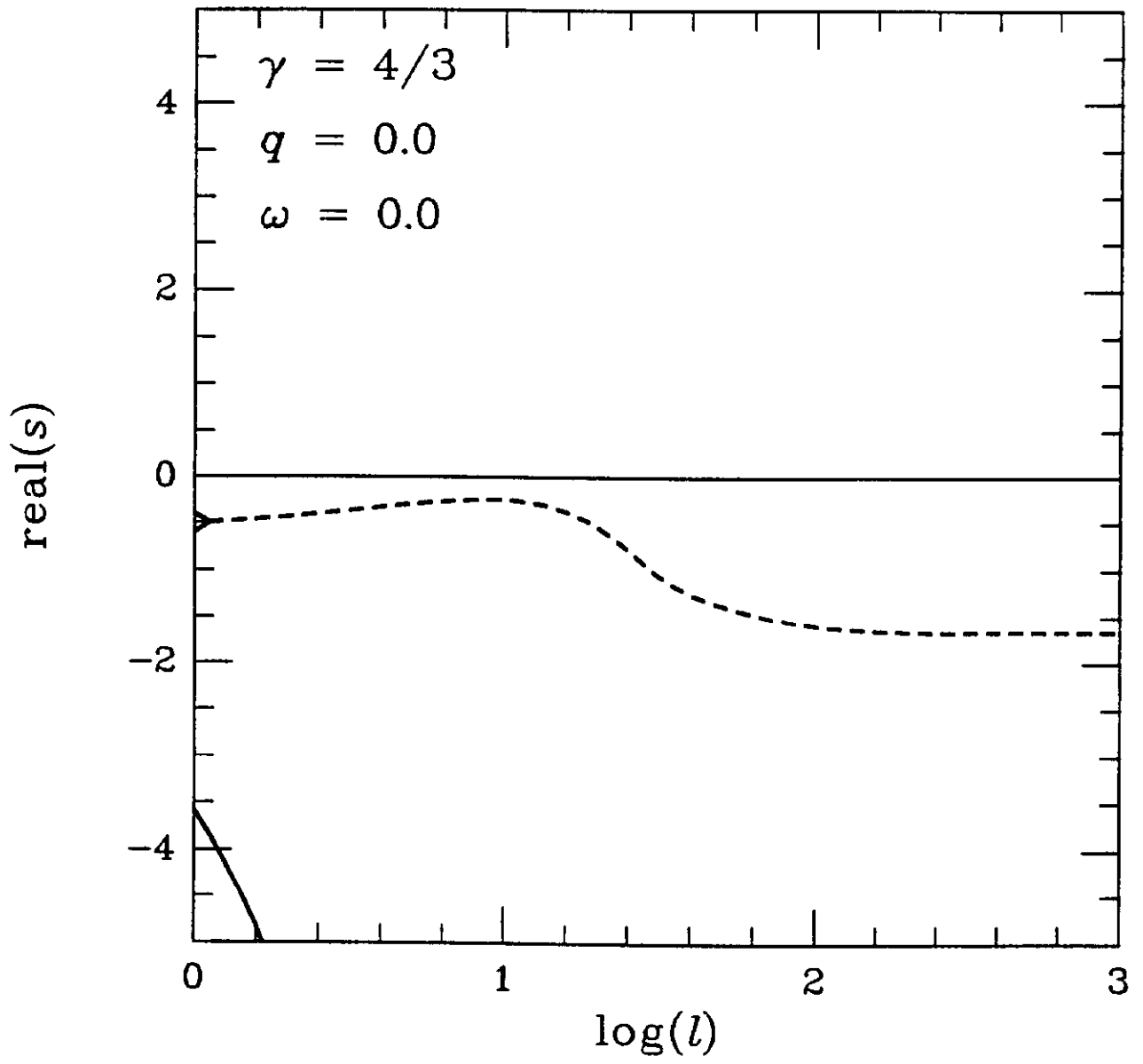


Fig 2a

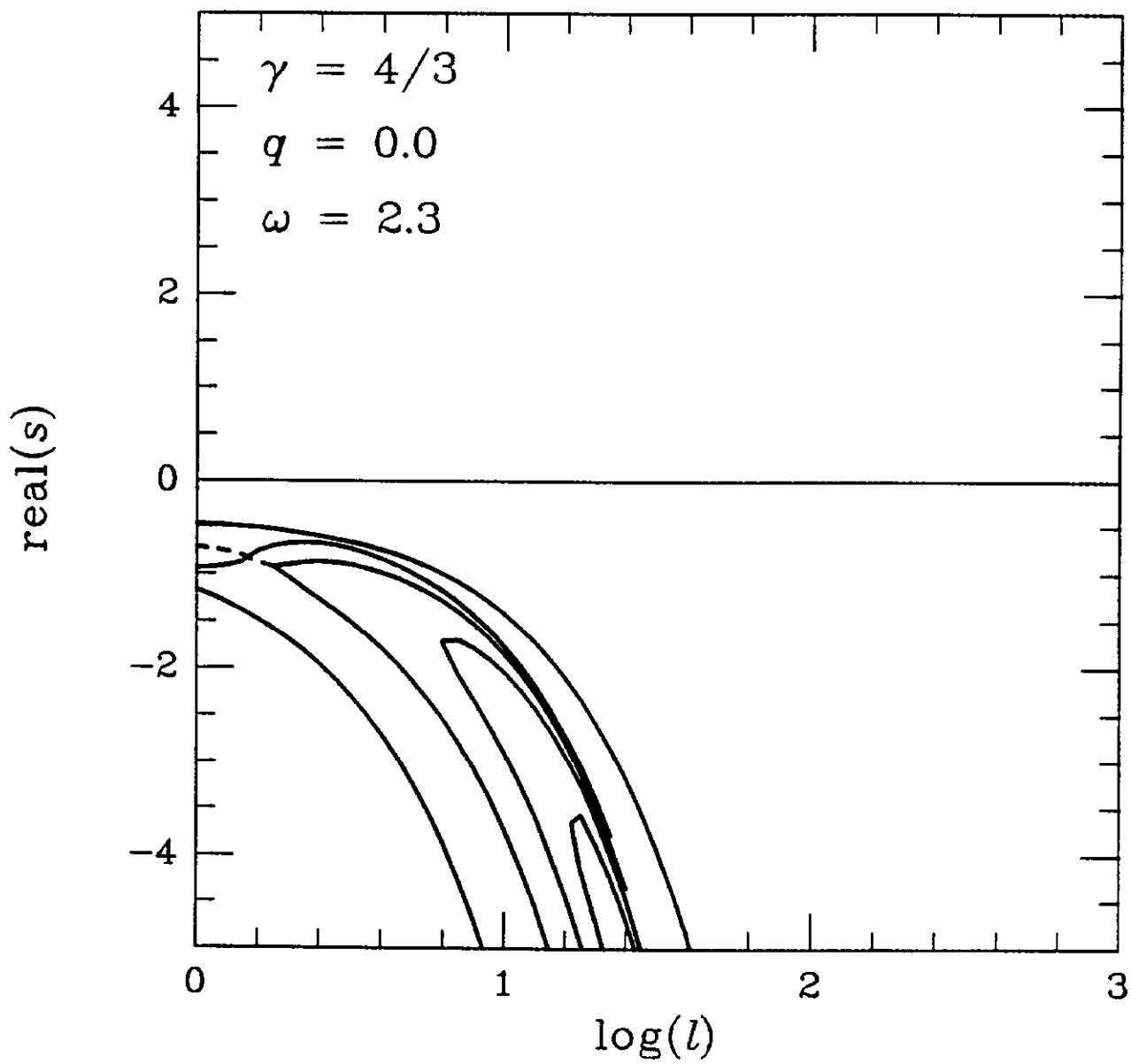
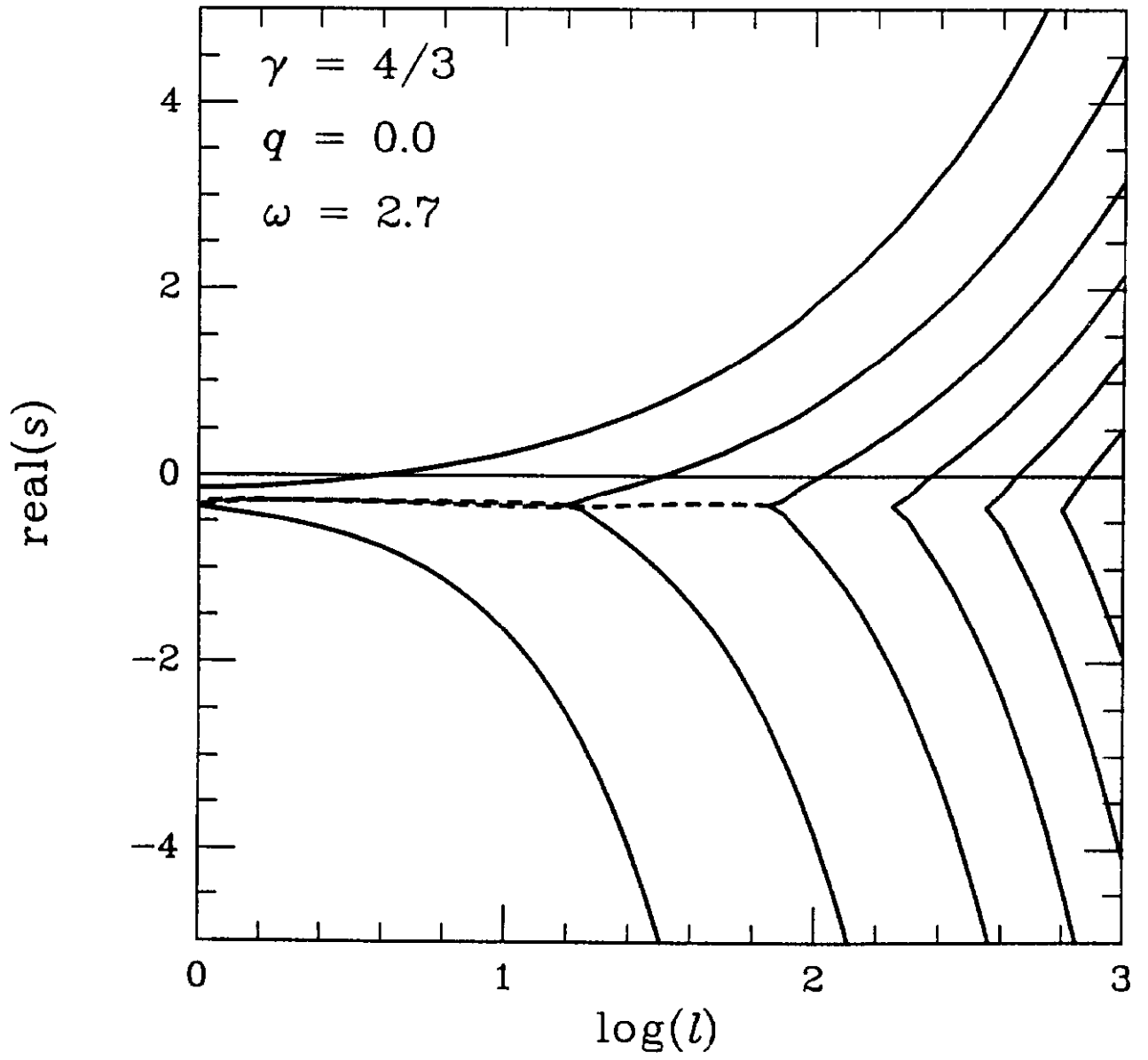


Fig 2b



Figure

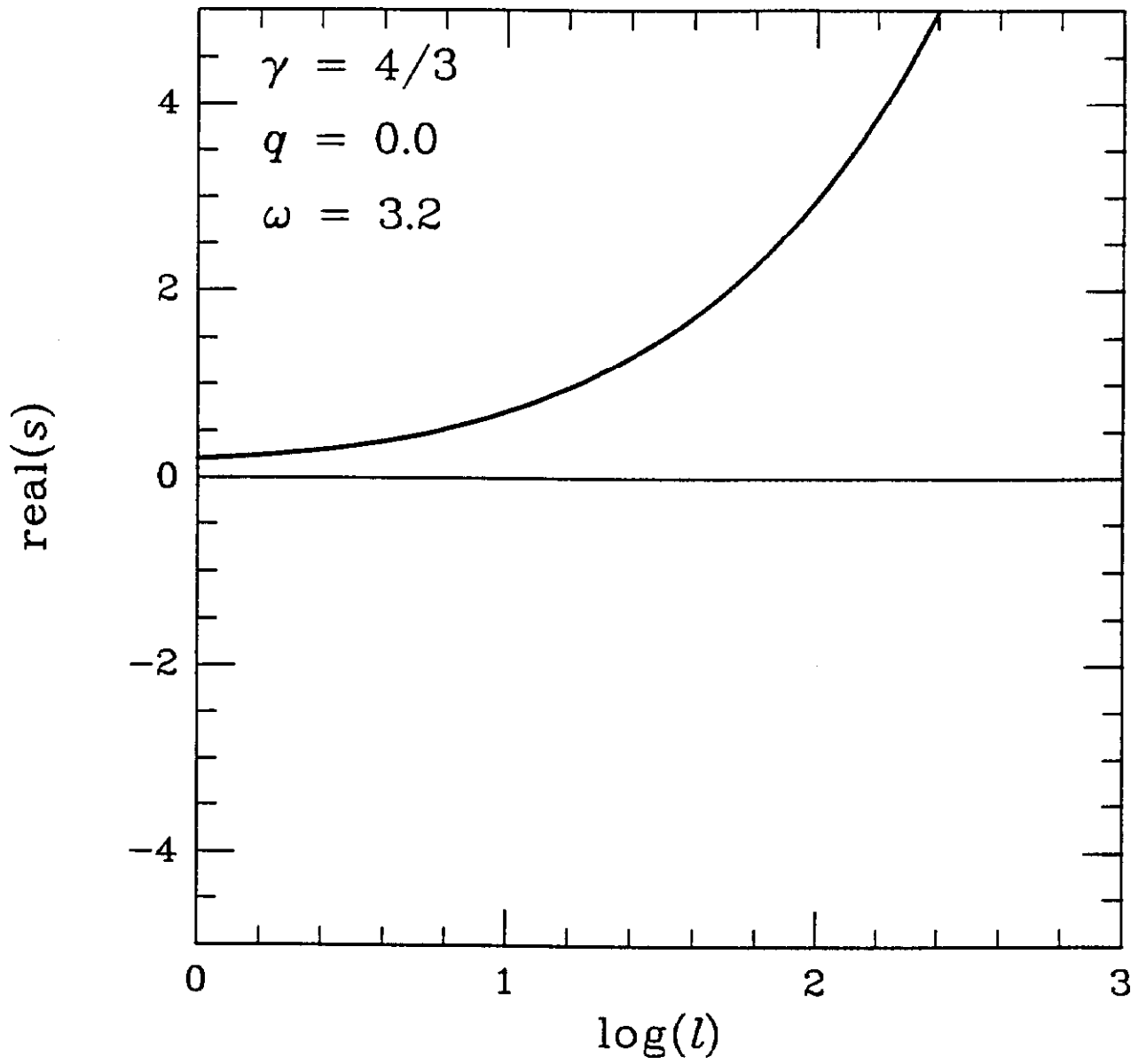


Fig 2d

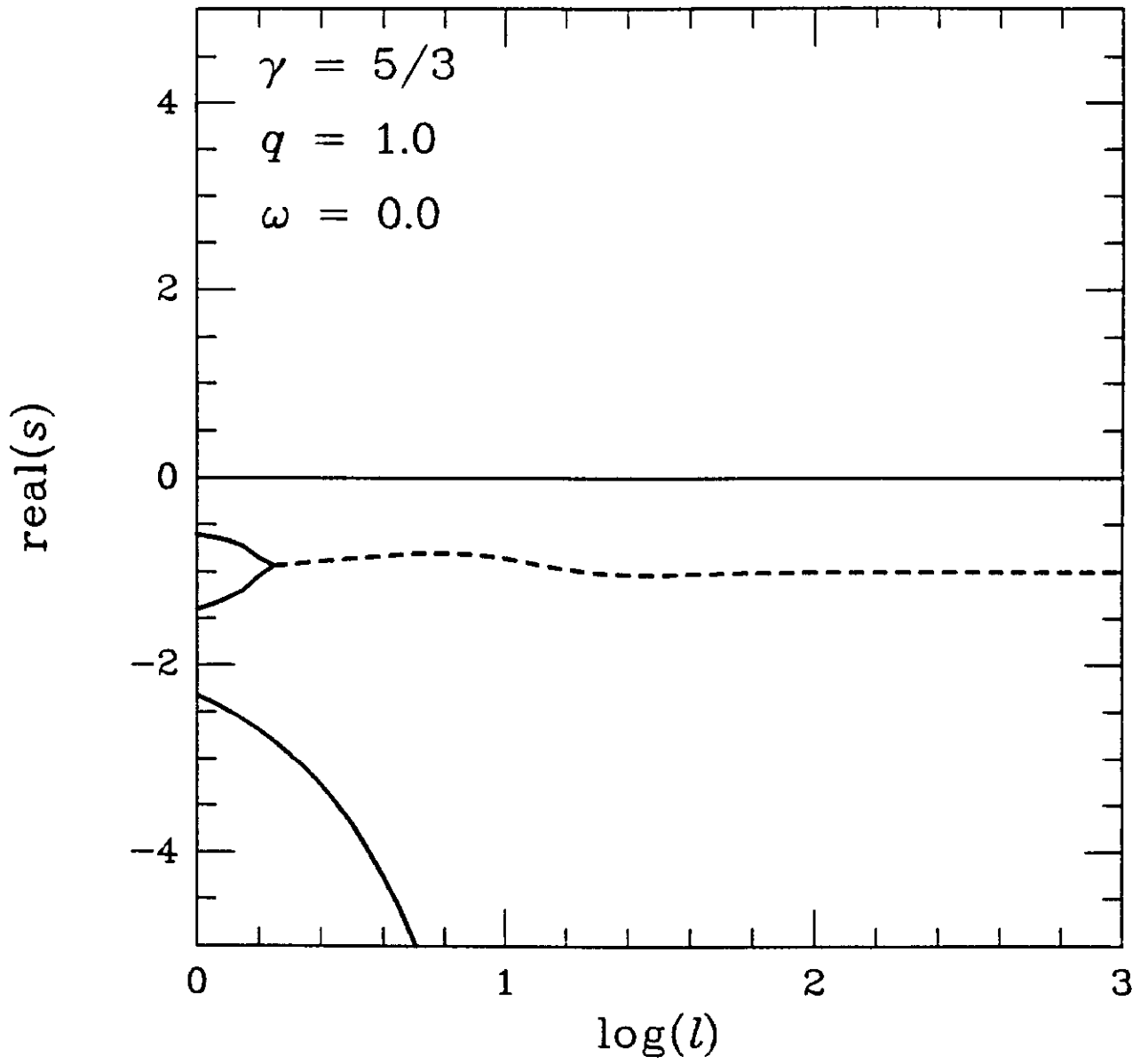


Fig 3a

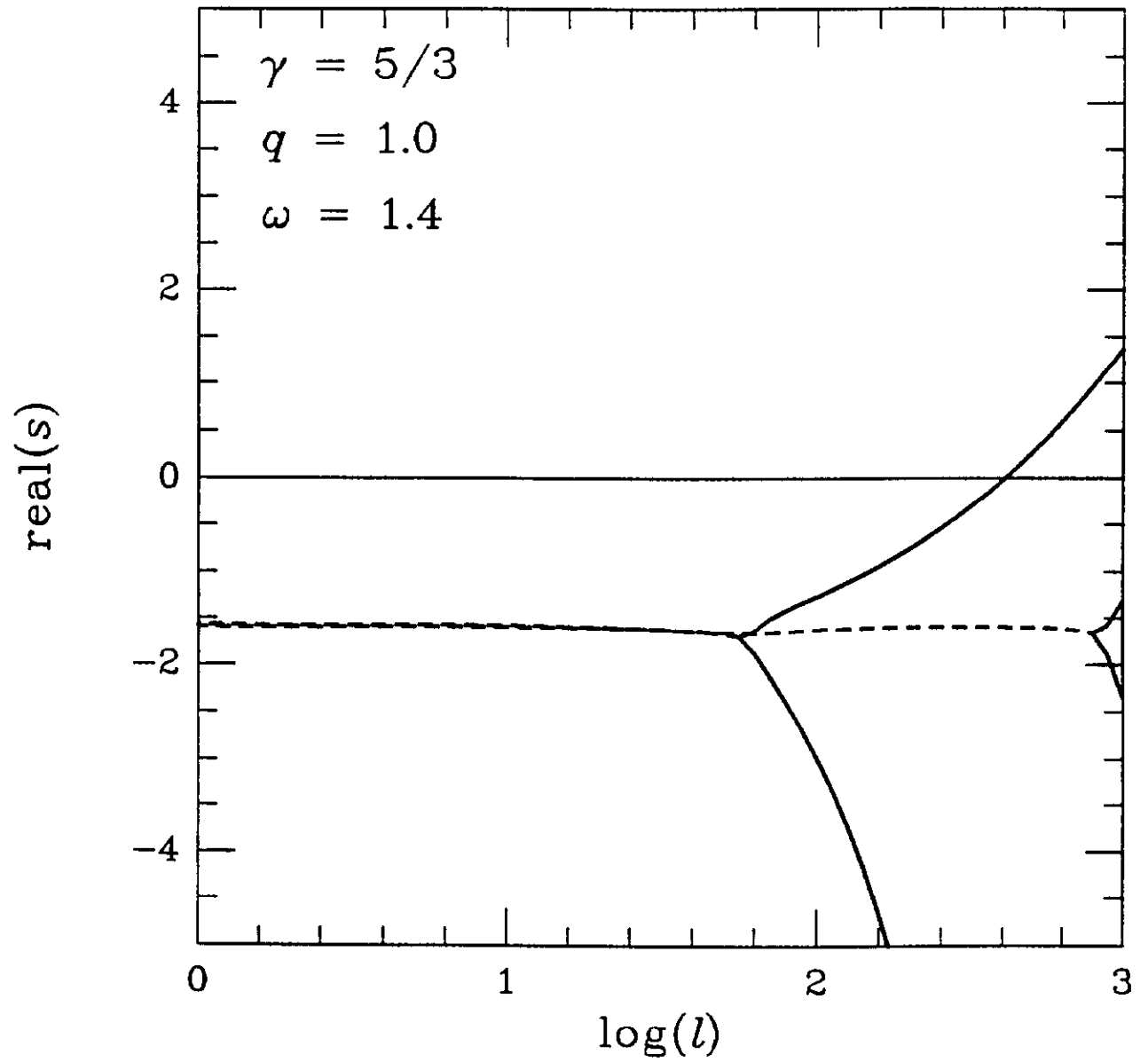


Fig 3b

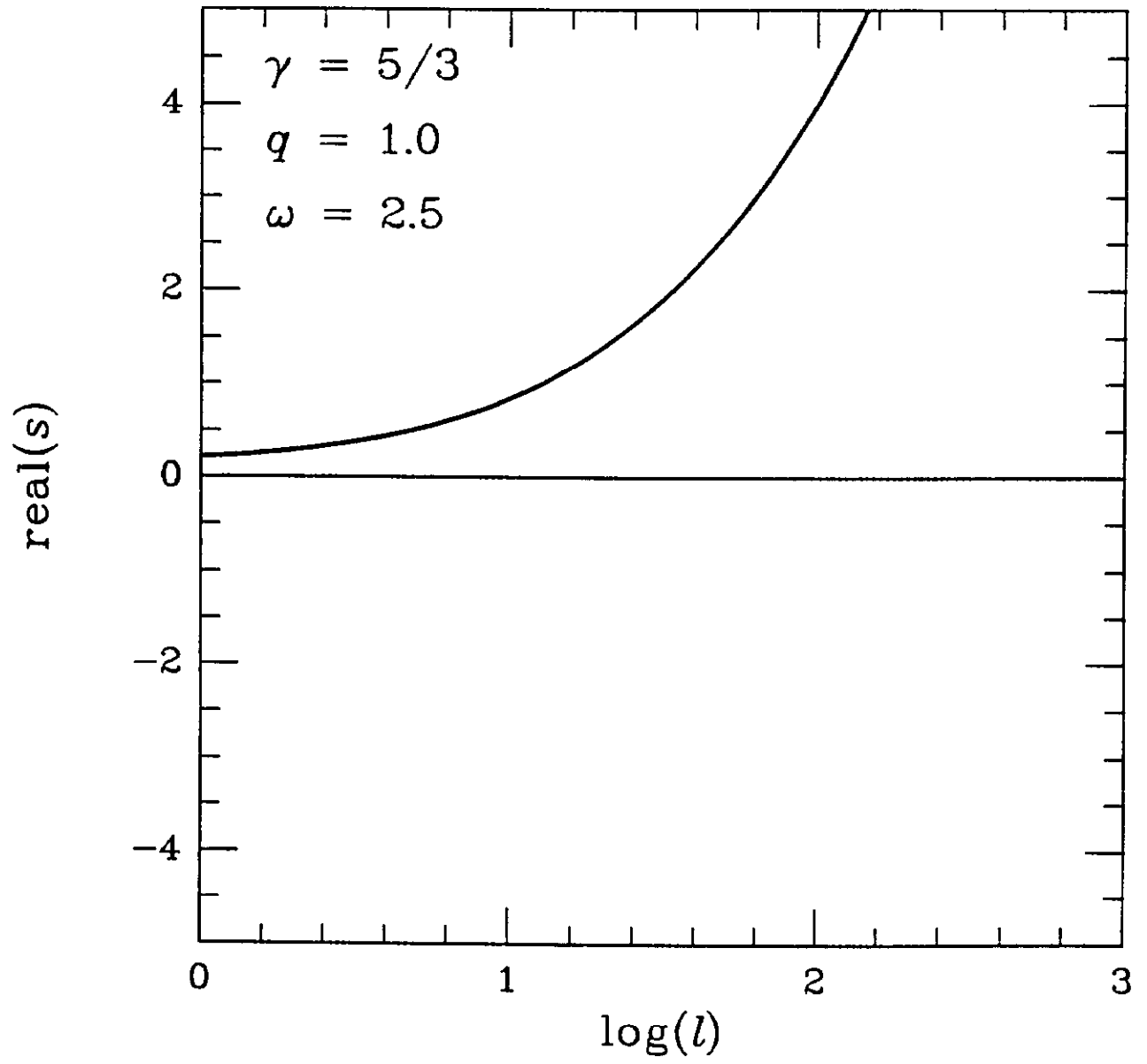


Fig 3c

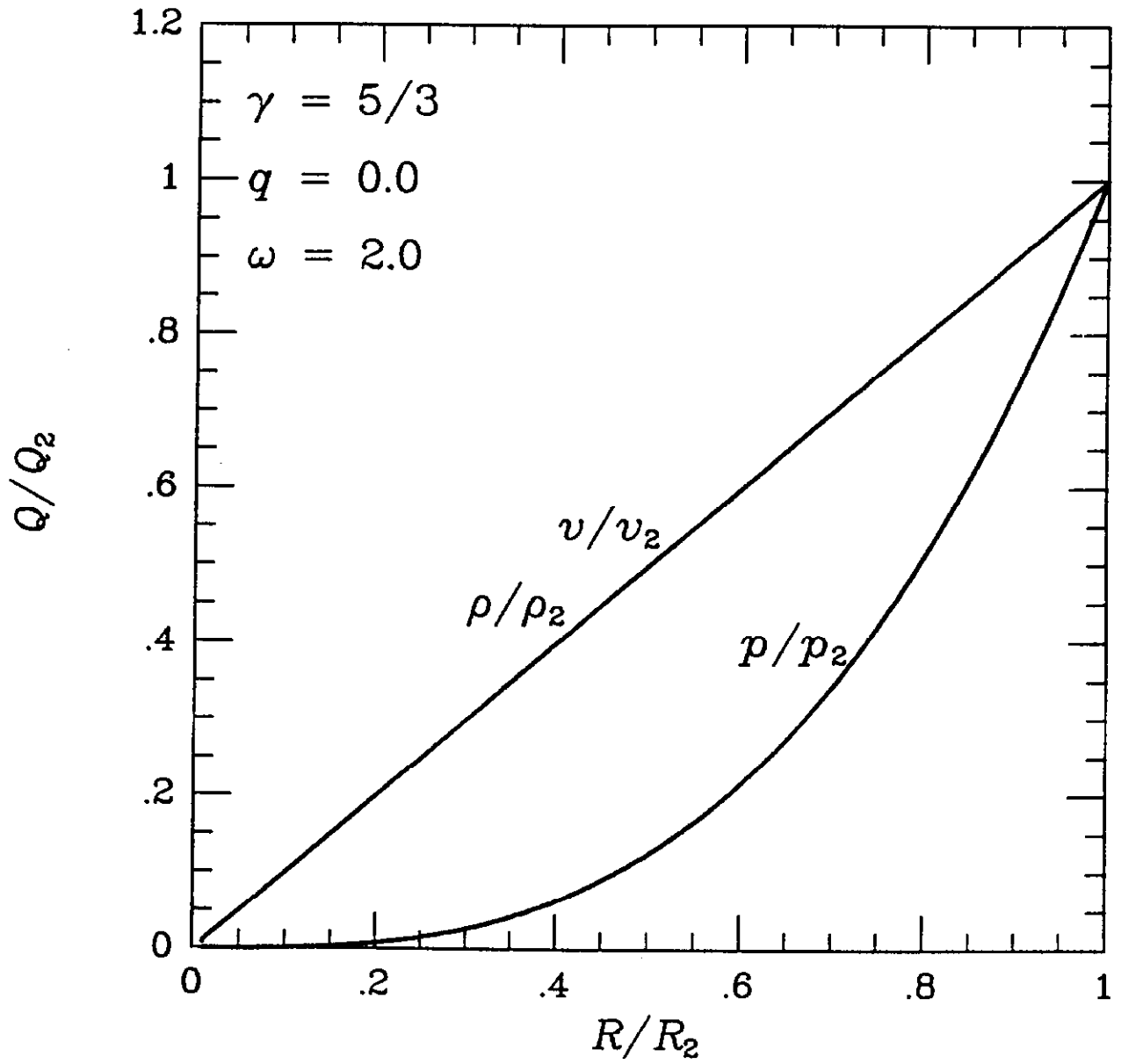


Fig 4a

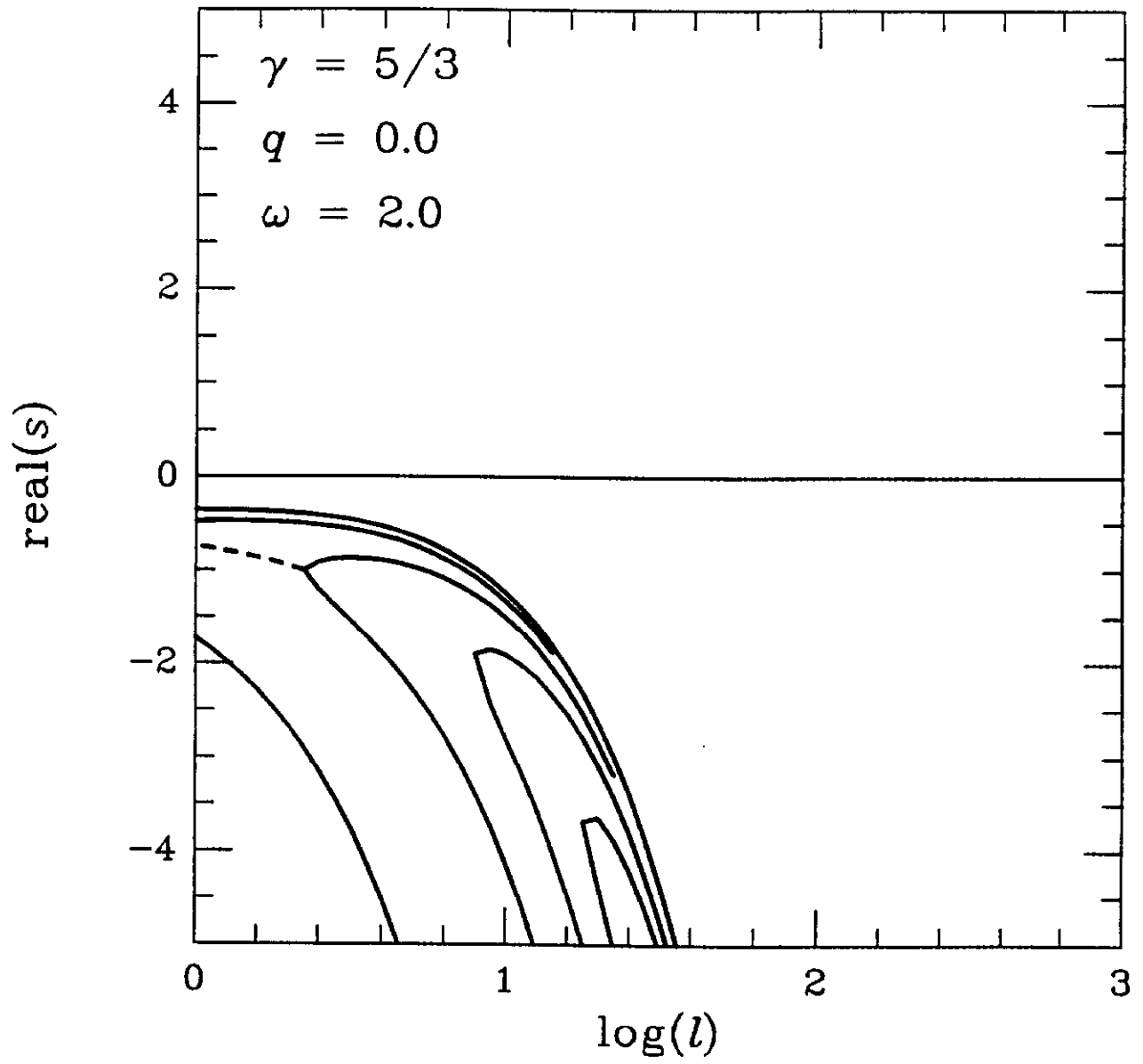


Fig 4b

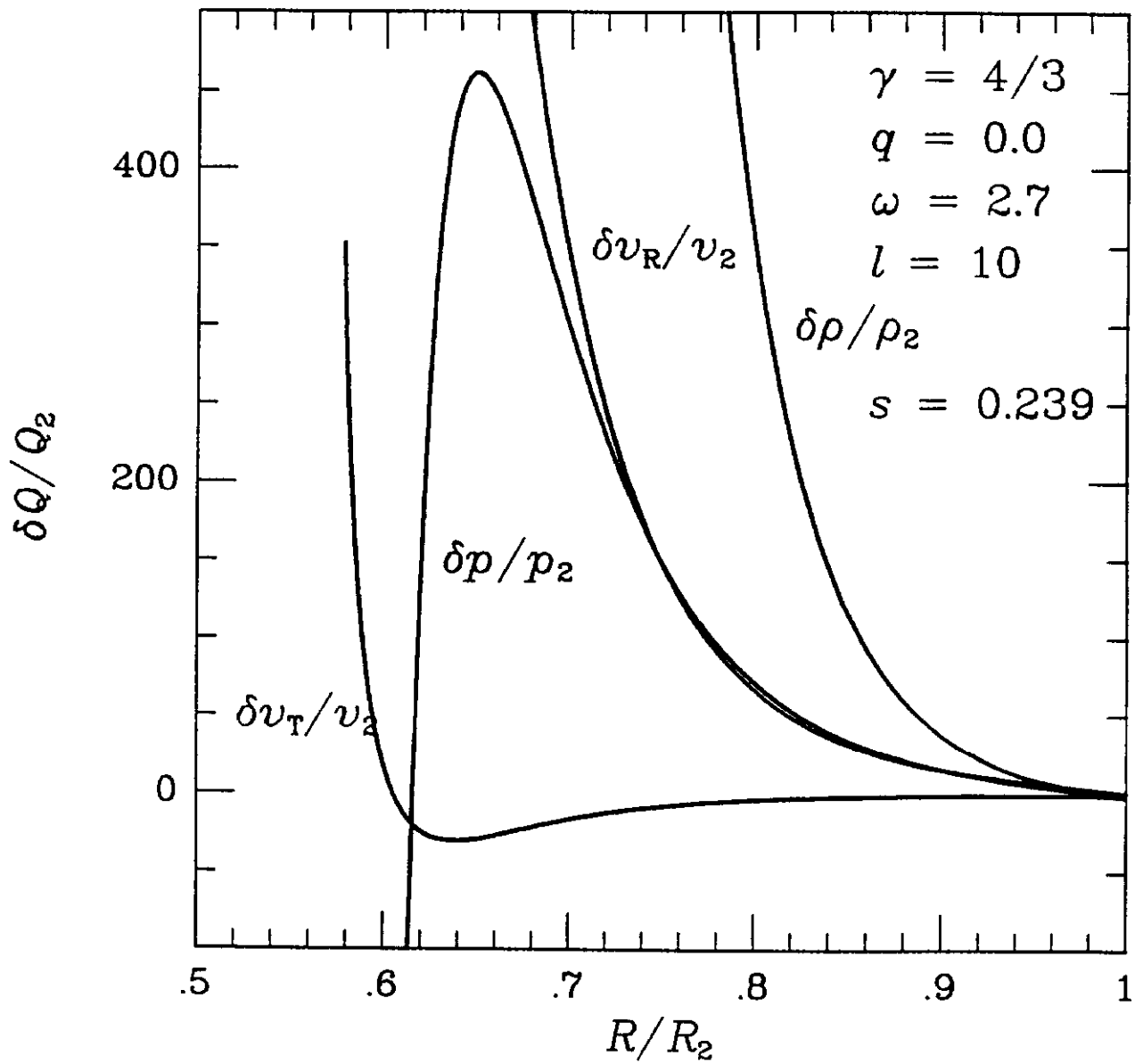


Fig 5a

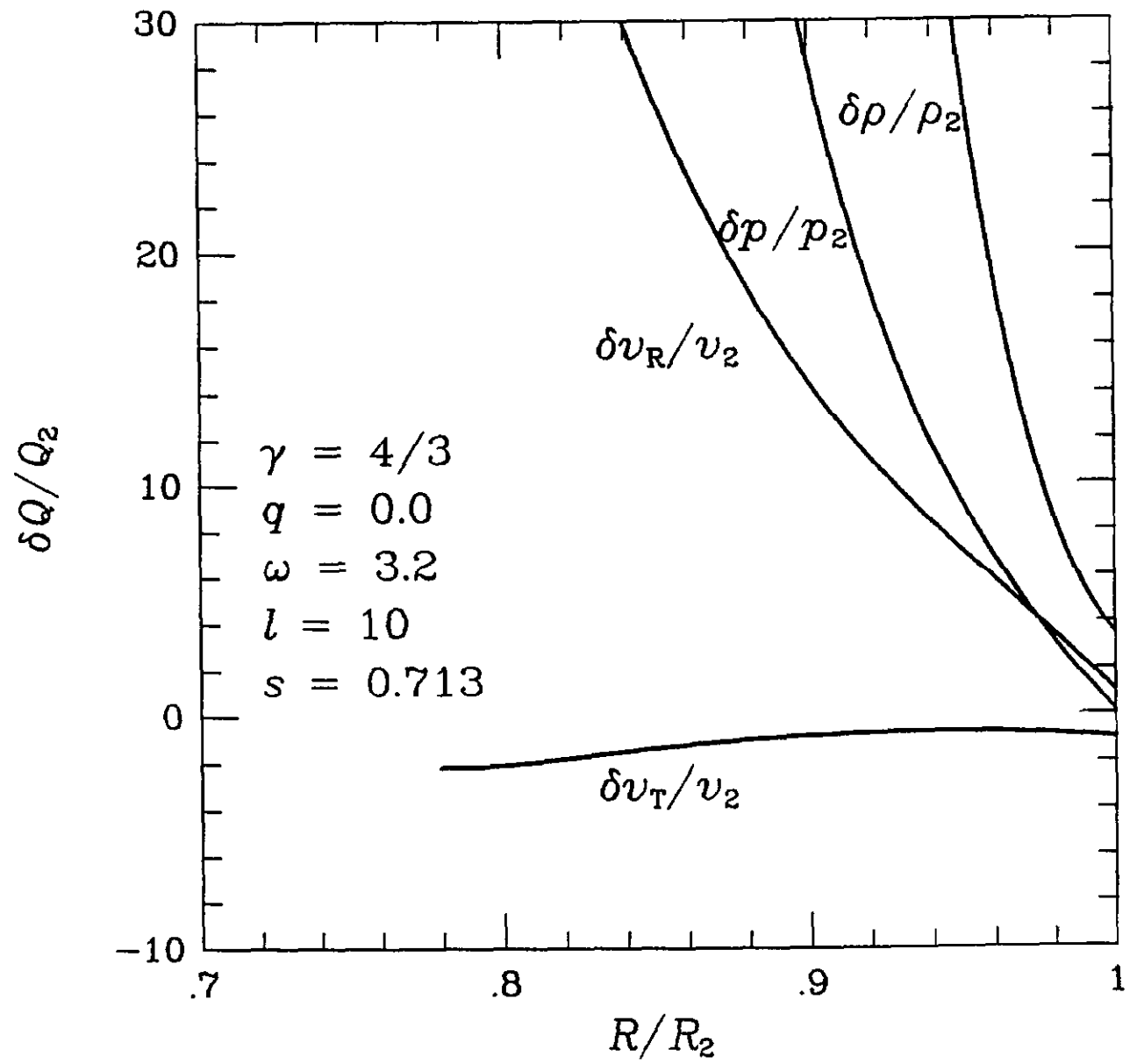


Fig 5b